University of Groningen

Bachelor Thesis

The small galaxies that built up the Galactic halo

Author:
Ines Berčuk

Supervisor:
Prof. E. Starkenburg
Second Examiner:
Prof. A. Helmi

Abstract

The Milky Way halo is thought to have been created as a result of many galactic mergers in the past. However, a qualitative analysis of its progenitors and their masses is still incomplete. In order to uncover the merger mysteries of the galactic halo, we use a novel statistical method (Deason et al., 2023) based on the mass-metallicity relation. This well-known relationship describes that more massive galaxies result in more metal-rich stars, while the opposite is true for less massive galaxies and metal-poor stars. Using a catalogue of stars on exclusively halo-like orbits (Viswanathan et al., 2023) with high-quality [Fe/H] measurements down to the extremely metal-poor regime (Martin et al., 2023), we probe even the smallest accreted galaxies in the formation history of the Milky Way halo. We find that the mass-spectrum of its progenitors is dominated by thousands of small galaxies with masses $\lesssim 10^5 M_\odot$, while we uncover only a few tens of progenitors with masses larger than this value and a single most massive galaxy with mass $\sim 10^8 M_\odot$. Using the mass-spectrum, we find the stellar mass of the halo of $(6.1 \pm 2.1) \cdot 10^8$ $M_\odot$. These findings bring us closer to disentangling the complete merger history of the Milky Way halo.

Contents

1 Introduction

It is currently understood that most of the stars in the Milky Way halo owe their origin to various other galaxies that merged with our own (see Helmi 2020 and references therein). As such, the galactic halo is quite literally a historical record of its encounters and a valuable region to study Galactic Archaeology. Furthermore, the galactic halo, along with the Local group, is one of the few regions of space where old stars are fully resolved. This greatly enhances the ability to study the formation of galaxies and disentangle their merger history.

In recent years, successful attempts have been made to decode the origins of stars that populate the halo using various methods. Helmi et al. (2018) and Belokurov et al. (2018) have shown that a massive progenitor named Gaia-Enceladus-Sausage (GES) merged relatively early with the Milky Way using demonstrations in velocity space, as well as found that the chemical abundances of these stars significantly differ from the rest of the galactic halo (see Deason and Belokurov 2024 and references therein). Before that, discoveries of the Helmi streams (Helmi and White, 1999) as well as disrupting stellar streams such as the Sagittarius (Ibata et al. 1994, Majewski et al. 2003) had already supported the hypothesis that the halo is formed as a result of past galaxy interactions. However, these few mergers do not fully disentangle the accretion history of the halo. Thus, the hierarchical structure of the outer component of the galaxy can be further decomposed by investigating the smaller galaxies that compose it. More recent works using Gaia data release 3 (DR3) supported by large spectroscopic surveys such as APO Galactic Evolution Experiment (APOGEE, Majewski et al. 2017) and Large sky Area Multi-Object fibre Spectroscopic Telescope (LAMOST, Zhao et al. 2012) show findings of numerous mixed and coherent stream-like substructures of both in-situ and accreted origin. Dodd et al. (2023) find several clumps and substructures in integrals of motion space in the local stellar halo, while most recently Ibata et al. (2024) use the `STREAMFINDER` algorithm to locate 87 stream-like structures out of which 28 are new discoveries. Hence, it is clear that identifying small-scale structures and dwarf galaxies is an important step in studying the formation of the Milky Way halo.

1.1 Mass-Metallicity relation

The metal content of a star is a chemical record of past star formation and gas dynamics of the galaxy as the star preserves the metallicity of its surroundings at the time of its formation for most of its lifetime. Hence, one way of investigating which dwarf galaxies merged with the Milky Way to create the galactic halo is to look into the chemical composition of stars in this region. A useful tool in this process is the mass-metallicity relation (MZR). This is an empirical relation that describes how the metal content of a galaxy changes as a function of its mass. Using spectroscopic metallicities of individual stars in 15 Milky Way dwarf spheroidal galaxies and 7 dwarf irregular galaxies in the Local Group, Kirby et al. (2013) find that the MZR for dwarf galaxies of the Milky Way (and the Andromeda galaxy or M31) is:

$$\langle [\mathrm{Fe/H}] \rangle = (-1.69 \pm 0.04) + (0.30 \pm 0.02) \log \left(\frac{\mathrm{M_*}}{10^6 \mathrm{M_\odot}} \right) \tag{1}$$

or simply $\mathrm{Z_*} \propto \mathrm{M_*^{0.30 \pm 0.02}}$. The term metallicity will be used to refer to [Fe/H][1] throughout this work.

Galaxies enrich themselves as a result of stellar evolution and supernova explosions that release

[1] $[\mathrm{Fe/H}] = \log\left(\frac{(\mathrm{N_{Fe}/N_H})_*}{(\mathrm{N_{Fe}/N_H})_\odot}\right)$

newly created metals into the interstellar medium of the galaxy. Because more massive galaxies have deeper gravitational potential wells than less massive ones, they are able to counteract processes such as supernova feedback and radiation pressure and maintain supernova ejecta more efficiently (Kirby et al., 2013). In addition to this, massive galaxies tend to produce stars at a faster rate compared to less massive ones (Davé, 2008). As a result, massive galaxies enrich themselves more quickly and create stars that are more metal-rich, while less massive galaxies create stars with relatively low metallicities. Remarkably, such a simple relation between mass and metallicity can encompass a complex balance between processes of inflow and outflow of gas in dwarf galaxies. Furthermore, it is important to note that this powerful relation is only locally established (Kirby et al., 2013) and is hence another advantage to studying the galaxy formation history of dwarf galaxies of the Milky Way. As mass and luminosity are closely related, the above expression can also be expressed in terms of luminosity:

$$\langle [\mathrm{Fe/H}] \rangle = (-1.68 \pm 0.03) + (0.29 \pm 0.02) \log \left(\frac{\mathrm{L_V}}{10^6 \mathrm{L_\odot}} \right) \tag{2}$$

We will use this relation accompanied by the statistical approach of Deason et al. (2023) to decompose the galactic halo into smaller accreted galaxies that compose it.

1.2 Reduced proper motion halo

The Gaia mission and its data releases have broadened the possible ways of studying the Milky Way thanks to a sample of over 1.8 billion stars (Gaia Collaboration et al., 2023). The so-called 6D sample with complete distance and velocity information has proven to be fruitful in studying the galactic halo and its merger history (Helmi et al. 2018, Koppelman et al. 2018 and Koppelman et al. 2019 amongst others), while the 5D sample of stars which lacks line-of-sight velocities is sometimes overlooked. This sample however comprises over 585 million sources (Gaia Collaboration et al., 2023), in addition to having accurate photometry and astrometry. Hence, it is worth exploring. Koppelman and Helmi (2021) have shown that the 5D Gaia sample can be used to create a sample of main sequence (MS) halo stars from Gaia DR2. Using a method known as the reduced proper motion (RPM), they avoid the use of distance and spectroscopic information and are able to identify these stars as halo stars on the base of Gaia proper motions and photometry. This is possible due to a strong, almost linear, relation between absolute magnitude and the colour of main sequence stars on the Herzprung-Russel (HR) diagram which allows them to express the absolute magnitude as a function of Gaia $\mathrm{G} - \mathrm{G_{RP}}$ colour. The RPM of a star, defined as $\mathrm{H_G}$, can be expressed in Gaia G-band in the following way:

$$\mathrm{H_G} = \mathrm{M_G} - 5 \log \left(\frac{\mathrm{v_{tan}}}{4.74057} \right) \tag{3}$$

where $\mathrm{M_G}$ is the absolute magnitude and $\mathrm{v_{tan}}$ is the tangential velocity of the star. By plotting the RPM as a function of colour for a stellar population, a diagram analogous to the HR diagram is obtained. Consequently, stars with similar values of tangential velocity group together and distinguish themselves into separate sequences. Under the assumption that disc stars have small tangential velocities compared to the halo stars, we can exclude them to create a sample of main sequence stars on halo-like orbits of the Milky Way. This approach also reduces the need to make additional distance cuts in order to ensure that only the halo stars are included in the sample which can result in the exclusion of actual halo stars located near the galactic plane. However, it should be noted that the RPM sample by definition excludes halo stars with tangential velocities close to those of the disc stars, so this method still imposes a dynamical bias towards high tangential velocity stars.

Following from Koppelman and Helmi (2021), Viswanathan et al. (2023) have created an even larger catalogue of about 47 million RPM main sequence stars by selecting high tangential velocity (200 km s^{-1} < v_{tan} < 800 km s^{-1}) stars in the MS colour range from the Gaia DR3. This sample has been cleaned by photometry and astrometry quality cuts and the magnitudes have been corrected for interstellar extinction (for further details we refer to Section 2 of Viswanathan et al. 2023). They use this catalogue to study low surface brightness components of stellar streams as they note that in addition to an almost linear relation between absolute magnitude and colour, the advantage of using MS stars to investigate the Milky Way halo lies in the fact that they largely outnumber any other type of star in this region simply due to the initial mass function. Furthermore, they are relatively long-lived and can therefore serve as snapshots in time of gas phase metallicity at the time of their formation. As the RPM method selects a pure MS sample, Viswanathan et al. (2023) also determine photometric distances using photometric parallax (Jurić et al., 2008), a colour absolute magnitude relation, with typical uncertainties as low as 2 %.

1.2.1 The Pristine Survey

One of the aims of this work is to decompose the Milky Way halo into smaller galaxies that once merged with our own. As mentioned previously, due to the MZR, the stars that compose these merger galaxies are likely metal-poor. Thus, the sample needed for our science has to include accurate and precise metallicities of halo stars down to the extremely metal-poor end ([Fe/H] < −3.0, Beers and Christlieb 2005). For this purpose, we will use the Pristine survey (Starkenburg et al., 2017). This is a narrow-band photometric survey that uses an almost top-hat filter centred around the Ca H&K doublet lines at 3968.5 and 3933.7 Å. It is located on the MegaCam imager at the Canada-France-Hawaii Telescope (CFHT). The filter is particularly efficient at detecting stars with low metallicities. This is evident from Figure 1 taken from Starkenburg et al. (2017) where the spectra of synthetic metal-poor stars are plotted at the wavelengths of the Ca H&K doublet lines which show weaker absorption features for metal-poor stars compared to more metal-rich ones.

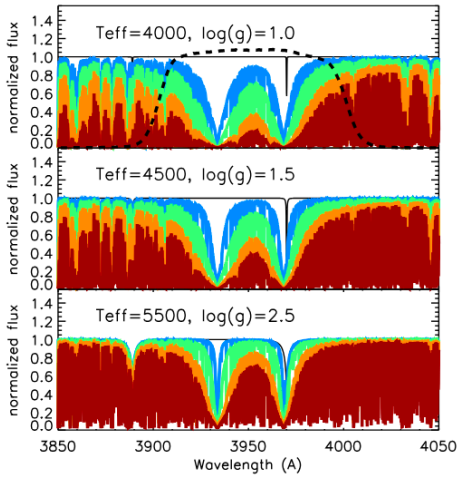

Figure 1: Figure 1. from Starkenburg et al. (2017): "Synthetic spectra using `MARCS` stellar atmospheres and the `TURBOSPECTRUM` code (...) of stars on three different places on the giant branch with metallicities [Fe/H] = 0.0 (red), [Fe/H] = −1.0 (orange), [Fe/H] = −2.0 (green), [Fe/H] = −3.0 (blue) and for a star with no metals (black). In the top panel the throughput of the Ca H&K filter used in Pristine is overplotted (black dashed line)."

As a result, the more metal-poor a star is, the brighter it will appear in this filter compared to more metal-rich stars with the same temperature and surface gravity in its surroundings, making it easier to detect. In other words, the measured photometric Ca H&K magnitude of a metal-poor star will be lower compared to a metal-rich star. Furthermore, as this method utilises photometry instead of spectroscopy, the Pristine survey can capture many stars with each measurement, unlike most spectroscopic methods which measure the spectra of stars in a serial manner. This greatly accelerates the ongoing search for very metal-poor stars in the Milky Way and is observationally more affordable. It is important to note that Ca H&K lines have a weak dependence on stellar parameters such as surface gravity apart from metallicity and temperature. However, as noted by Starkenburg et al. (2017) these dependencies can be ignored for metal-poor stars in the first hand approach.

In order to acquire photometric metallicities, the first version of the Pristine survey relied on Sloan Digital Sky Survey (SDSS, Abolfathi et al. 2018) in order to calibrate its photometry (Starkenburg et al., 2017). This approach has since been adapted to use the Gaia broadband photometry (Martin et al., 2023). We will outline their approach here. Firstly, the sample is de-reddened and contaminants such as variable stars are removed. In order to create a scale that relates the magnitude of a star and its Pristine magnitude, Martin et al. (2023) create a spectroscopic training sample composed of SDSS, Sloan Extension for Galactic Understanding and Exploration (SEGUE, Yanny et al. 2009) and APOGEE stars, in addition to adding known ultra metal-poor (UMP, [Fe/H] < -4.0), extremely metal-poor (EMP, [Fe/H] < -3.0) and very metal-poor (VMP, [Fe/H] < -2.0) stars that were otherwise missing from the aforementioned catalogues. The stars in the training sample are selected such that they appear as point sources in the Pristine observations and have precise photometry with photometric uncertainties δCa H&K smaller than 0.05. It is important to note that this training sample includes FKG stars only, as hotter stars show too faint Ca H&K lines, while colder stars have lower continuum which also hampers the measurement of the required absorption lines. Using the four magnitudes in the sample (Ca H&K, G, G_{BP} and G_{RP}), a colour-colour space is constructed with $(\text{Ca H\&K} - \text{G})_0 - 2.5(G_{BP} - G_{RP})_0$ on the y-axis and $(G_{BP} - G_{RP})_0$ on the x-axis (Martin et al., 2023). The space is divided into smaller cells for which an average metallicity of training sources occupying each cell is calculated. This training colour-colour grid is then used to determine the metallicities of the stars in the Pristine footprint based on their location in the grid. The resulting catalogue of photometric metallicities is very well suited for our study of metal-poor stars in the Milky Way halo (as demonstrated by Youakim et al. 2017, Aguado et al. 2020 and Viswanathan et al. 2024). The catalogue provides two metallicity solutions for each star: for a dwarf and a giant. As our catalogue is composed of MS halo stars, we proceed using the dwarf photometric metallicities.

1.3 Mass-spectrum of destroyed dwarf galaxies

In order to study the evolution history of the Milky Way, or more precisely the halo, an important ingredient is the mass spectrum of its likely many progenitors. Deason et al. (2023) have recently introduced a new statistical method that can find this necessary component. We will briefly summarise their work here. As described above, many progenitors of the Milky Way have been discovered with the use of Gaia 6D information in velocity-space, however, disentangling this data can pose a major challenge. Fortunately, there is an alternative way of searching for potential merged galaxies using the chemical composition of stars by virtue of the MZR shown in eq. 1. This approach has not been widely explored, until recently. Deason et al. (2023) created a method that employs an unbinned MDF of a galaxy or its region. This way, using the MDF

of an accreted stellar population, we can uncover the mass-spectrum of its progenitors.

This statistical approach uses a sample of metallicity measurements from a given region of stars along with an estimate of its total luminosity to decompose the MDF into smaller accreted components, i.e. into masses or luminosities of smaller galaxies that could have composed that region. It is based on the LZR (eq.2) found by Kirby et al. (2013). The model employs `dynesty` (Speagle, 2020), a Python package for nested sampling, to reiterate over the sample until maximum likelihood is reached. At this point, it decomposes the overall MDF into a mixture of MDFs of smaller galaxies and returns the number of accreted galaxies along with their luminosities. It is important to note that the key assumption of this model is that the MDF of a galaxy can be approximated as a mixture of MDFs of the smaller galaxies that compose it, where the MDFs of the smaller galaxies can be approximated as Gaussian functions.

Deason et al. (2023) compute the luminosity spectra of the Milky Way halo as well as the classical Milky Way satellites. As the topic of interest of our work is the halo, we will focus on this component of the results. They use a combined sample of multiple spectroscopic surveys combined with photometric distances from Gaia DR3 and quality cuts that select halo stars in the Milky Way. They decompose the halo using two different MZRs: the Kirby et al. (2013) MZR (eq. 1), as well as one with an offset of -0.3 dex to this relation, as it is postulated by Naidu et al. (2022) to be more suitable for destroyed dwarf galaxies, as opposed to surviving ones. For both relations, they find about 400 progenitors with $M_V \gtrsim -10$ but with varying mass-spectra. Moreover, using the Kirby et al. (2013) MDF they find 1 progenitor galaxy with luminosity $\approx 10^{8.5}$ $L_\odot$, while this number rises to 3 when using the Naidu et al. (2022) offset to lower metallicities. As a result of the simulations, they also uncover additional estimates of the halo luminosity: $1.1^{+0.2}_{-0.2} \cdot 10^8$ $L_\odot$ for Kirby et al. (2013) MDF and $3.4^{+7.2}_{-2.3} \cdot 10^8$ $L_\odot$ for -0.3 dex offset to the MDF. Furthermore, they test their method on 28 simulations of galaxies with the mass of the Milky Way halo and find that their MDF decomposition works well, i.e. that they can uncover the true mass-spectrum within 50 % for most luminosity bins. However, they do note that the number of low-mass accreted galaxies tends to be overestimated, likely because of the assumption of the Gaussian MDF of a galaxy, which is unlikely to hold as galaxies tend to have longer tails in the metal-poor regime (Leaman, 2012).

1.4 Aims

In this work, we set out to disentangle the rich merger history of the Milky Way by finding the mass-spectrum of its progenitors and performing an additional metallicity analysis of components of the halo. We will combine the statistical MDF decomposition method (Deason et al., 2023) with the high-quality metallicity measurements from the Pristine photometric survey (Martin et al., 2023) for galactic halo stars selected by the RPM catalogue (Viswanathan et al., 2023). With the introduction of this catalogue, we acquire a homogeneous [Fe/H] sample that probes the smallest scale dwarf galaxies that created the halo. In addition to this, we will test the robustness of the results of the decomposition method when the halo is approximated by only a portion of itself. We start by describing the catalogue of stars, the methods to explore their chemical composition and determine the mass-spectra of their merger galaxies in Section 2. We present the results of these methods in Section 3 and discuss their implications, drawbacks and further work in Section 4. Finally, in Section 5 we outline our approach and present the main findings.

2 Methods and Data

2.1 Observational data

In order to create a sample of MS halo stars with high-quality values of metallicity required for our science, we cross-match the sources from the RPM halo catalogue from Viswanathan et al. (2023) to DR1 and deeper proprietary data from the Pristine survey (Martin et al., 2023) and consequently improve the photometric distances of the corresponding halo MS metal-poor stars. This reduces the number of sources in our sample, but greatly improves the metallicty accuracy. It allows us to more precisely decompose the metallicity distribution function (MDF) at different heights from the galactic plane, thereby uncovering possible stellar streams and past mergers hiding in the galactic halo.

2.1.1 Completing the catalogue

In order to complete the cross-matched catalogue to fully suit our science, we add additional columns. Firstly, in order to explore different regions of the galactic halo, we want to express the locations of stars with respect to the centre of the galaxy. Therefore, we calculate the galactic longitude l and latitude b using the Gaia DR3 celestial coordinates. Furthermore, using the photometric distance from Viswanathan et al. (2023) computed using Pristine metallicities, we find the Cartesian coordinates of stars with respect to the Sun and scale them to be with respect to the centre of the Milky Way. This allows us to divide the galactic halo into different regions based on the height from the galactic plane. Secondly, we estimate the uncertainty in photometric metallicity using parameters `FeH_Pristine_dw_84th` and `FeH_Pristine_dw_16th` which correspond to the 84th and 16th percentile of the probability distribution function (PDF) of the photometric metallicity estimate for dwarf stars:

$$\delta\text{Ca H\&K}_{\text{phot}} = 0.5 \cdot (\texttt{FeH\_Pristine\_dw\_84th} - \texttt{FeH\_Pristine\_dw\_16th}) \tag{4}$$

2.1.2 Quality cuts

Furthermore, we apply quality cuts to the data set as recommended by Martin et al. (2023) and Viswanathan et al. (2023) in order to ensure accuracy and precision. They are described below.

1. We only include stars with $-4.0 < [\text{Fe/H}] < 0.0$ in order to remove the buildup of sources near the edges of the metallicity grid.

2. We exclude the sources with the parameter `mcfrac` smaller than 0.8. This parameter describes the fraction of Monte Carlo samplings of the magnitude uncertainties that fall outside the model colour space (Martin et al., 2023), therefore we include only those sources that are within the range at least 80% of the time.

3. We include stars with photometric uncertainty δCa H&K < 0.5 dex. A cut of δCa H&K < 0.3 dex is also suggested, however, we opt for the less conservative one in order to sample a larger number of stars.

4. As recommended, we use $P_{\text{var}} < 0.3$ to remove potential variable stars as well as Gaia astrometry quality cuts for re-normalised unit weight error `RUWE` < 1.4 and $|$`Cstar`$|$ < `Cstar_1sigma` which ensures that that the Gaia corrected flux excess is within one standard deviation of itself.

5. In order to ensure that the sources in the catalogue are detected by Pristine as very likely stars (`merged_casu_flag` $= -1$) or likely stars (`merged_casu_flag` $= -2$), we impose a cut on the parameter `merged_casu_flag` and include only the sources with values -1 or -2.

6. Viswanathan et al. (2023) have already placed a cut of $\log\left(\frac{\mathrm{H_G}}{\delta \mathrm{H_G}}\right) > 1.75$. This cut filters the sources whose reduced proper motion (eq.3) is at least $10^{1.75}$ times larger than its error. It therefore only selects stars with reliable RPM.

7. Lastly, a cut of $0.45 < \mathrm{G_0} - \mathrm{G_{RP,0}} < 0.715$ is placed. It excludes turn-off and redder stars that do not completely follow the relation between absolute magnitude and the colour of main sequence stars mentioned in Subsection 1.2.

After applying all the said cuts, our sample is left with 294,015 stars out of the initial 1,314,160. While this reduced the amount of available sources by almost 80%, it ensures great quality and accuracy of the data, consequently improving the quality of the results. Figure 2 shows the footprint of the final catalogue in galactic coordinates. The plots shown in galactocentric coordinates throughout this work are plotted such that negative longitudes are on the left side of the figures and positive longitudes are on the right. Hence, we warn about the interpretation of the figures, as the Milky Way is usually projected mirrored to this.

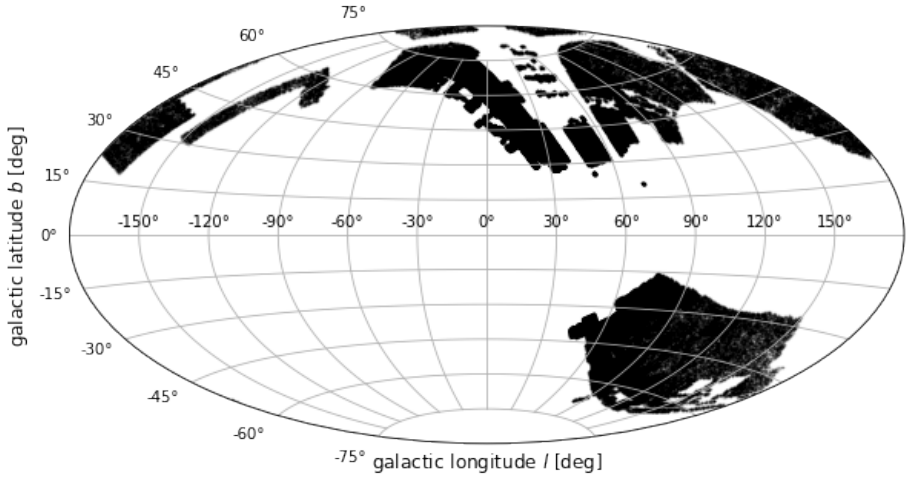

Figure 2: Footprint of the final catalogue based on the Pristine DR1 (Martin et al., 2023) and RPM catalogue (Viswanathan et al., 2023) with applied quality cuts described in 2.1.2.

2.2 Gaussian Mixture

To begin our study of the Pristine DR1 and PRM catalogue, we first investigate the metallicity composition of the halo and its components by fitting multiple Gaussian functions to it. This way we can more thoroughly probe the chemical composition of various parts of the halo and see how they differ from one another. This also allows us to further interpret the mass-spectra of different regions of the halo. In order to do this, we divide the halo into 33 regions based on galactic latitude b and longitude l in such a way that most regions have about 10,000 stars, to avoid the statistics of small numbers while still creating a significant amount of division. The regions are shown and labelled in Figure 3.

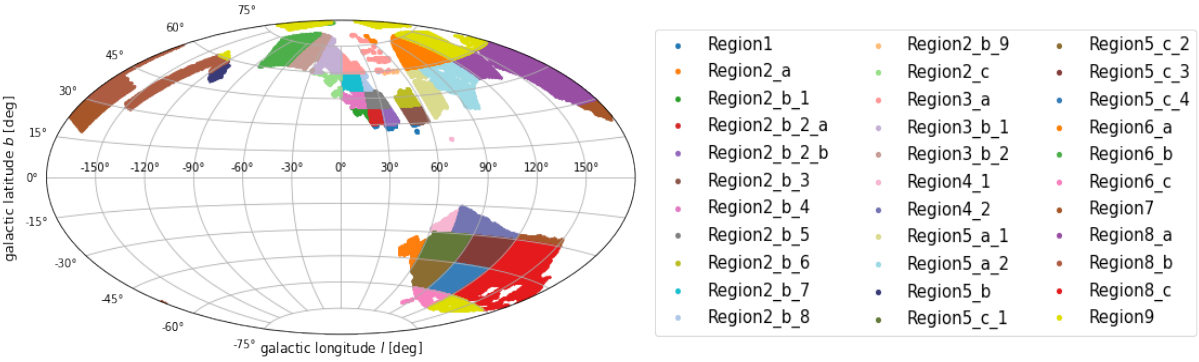

Figure 3: The total halo catalogue divided into 33 regions based on galactic latitude b and longitude l.

In order to fit multiple Gaussian functions to each region, we use a piece of code made by A. Viswanathan (priv. comm.) and slightly alter it to better suit our science. The code implements a `GaussianMixture` module from a Python `sklearn.mixture` package (Pedregosa et al., 2011) which estimates the parameters of a Gaussian mixture distribution. The model is based on an expectation-maximisation algorithm that assumes random components at the start and through an iterative process reaches the maximum likelihood of fit. It uses the metallicity distribution of a given sample to fit an overall curve to it as well as fit multiple Gaussian probability distribution functions to the data. The module is allowed to fit between 1 to 10 Gaussian functions to the given data and assigns the best fit Gaussian mixture based on the lowest Bayes information criterion. The approach results in a plot similar to the one in Figure 4. This figure shows the Gaussian decomposition of the entire halo catalogue along with the three fitted regions of the halo and the corresponding means.

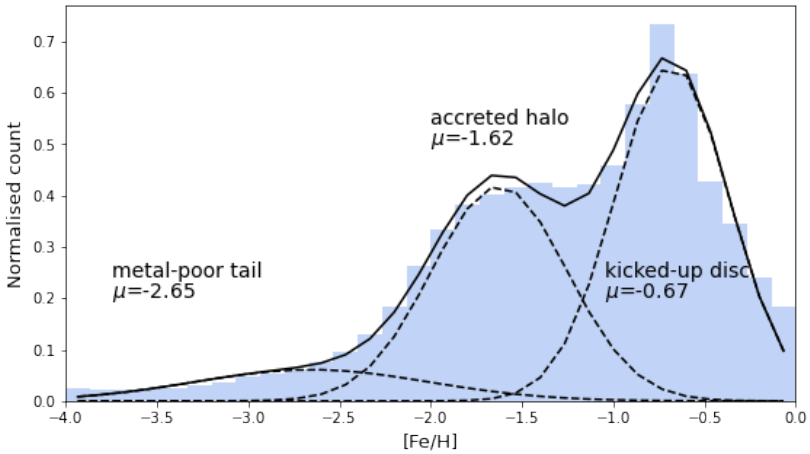

Figure 4: Gaussian mixture fitted to a histogram of metallicities of stars in the combined Pristine DR1 and RPM catalogue. The y-axis represents the normalised count of stars such that the total integrated probability is one, while the x-axis shows the metallicity of each bin. The three dotted lines represent the probability distributions of the three fitted Gaussian functions while the full line is the summation of the other three. Each curve is attributed a mean, which is also shown in the plot along with the name of three components of the halo we find.

In most cases, three Gaussian distributions can be fitted to the overall MDF of a given region. The most metal-rich peak can be interpreted as a thick disc component that includes the stars that were kicked up in the halo by the GES merger approximately 10 Gyr ago (Helmi et al. 2018, Belokurov et al. 2020), we further elaborate on this component in 3.1. The second Gaussian likely corresponds to an accreted component of halo stars, while the most metal-poor peak represents the metal-poor tail of stars, likely brought into the Milky Way by small-mass galaxies. We use this interpretation to create plots of the entire halo catalogue divided into the 33 regions shown above and investigate their mean metal content. The results of this approach are shown in 3.1.1.

Additionally, we perform an analysis of the fraction of stars belonging to each of the three components of the halo catalogue described above for each region. Using the results of the Gaussian decomposition, we integrate the PDF of each individual Gaussian component to acquire the fraction of stars belonging to it. We then create plots colour-coded for the percentage of stars and show the result in 3.1.2.

2.3 Metallicity distribution function decomposition

In order to decompose the metallicity distribution function of the halo stars, we use the generative model presented by Deason et al. (2023) described in 1.3. As mentioned earlier, the main assumption of this approach is that the MDF of a galaxy can be represented as a mixture of Gaussian MDFs of smaller galaxies, this allows for simpler decomposition of the sample but can also affect the results, we discuss this point further in Subsection 4.3. In addition to the metallicity sample and overall luminosity mentioned above, the main function of the metallicity decomposition model allows for the input of additional parameters that guide the simulation. All the used parameters are described in 2.3.1.

2.3.1 Setup of the simulation

As mentioned previously, the sample of metallicities is adopted from a cross-match of the RPM halo catalogue of Viswanathan et al. (2023) to DR1 and deeper proprietary data from the Pristine survey (Martin et al., 2023) completed with the aforementioned quality cuts. For the approximate luminosity of the halo, we adopt the value of $(7.9 \pm 2.0) \cdot 10^8 L_\odot$ from Deason et al. (2019). This value is found to be the luminosity of the Milky Way halo excluding the Sagittarius stream. In literature, the Sagittarius stream is located somewhere from 24 kpc to 28 kpc from the galactic centre (Vasiliev et al., 2021). Our data probes the stars to a distance of about 20 kpc from the centre, therefore it is reasonable to conclude that the Sagittarius stream does not pollute our data. However, we do note that there are older wraps of the stream that come much closer. In order to ensure that our use of the lower luminosity is justified, we perform an additional check using the model particles of the Sagittarius galaxy in the potential of the Milky Way and the Large Magellanic Cloud (LMC) by Vasiliev et al. (2021). We place a cut on the galactocentric distance such that stars further than 20 kpc away are not included, as this is the distance our catalogue probes. In Figure 5, we show the complete simulation of the Sagittarius galaxy in the left panel colour-coded by galactocentric distance and over-plotted on our catalogue, while in the right panel, we show a part of the galaxy that spans the distance range spanned by our catalogue, colour-coded by stripping time. It is clear that most of the Sagittarius stars do not belong to our catalogue, however, we do see that part of the stars belonging to the older wrap of the galaxy (in purple) could be included in our sample. Nevertheless, they comprise a small fraction of the total stars belonging to the stream, so we conclude that our use of the lower luminosity is justified.

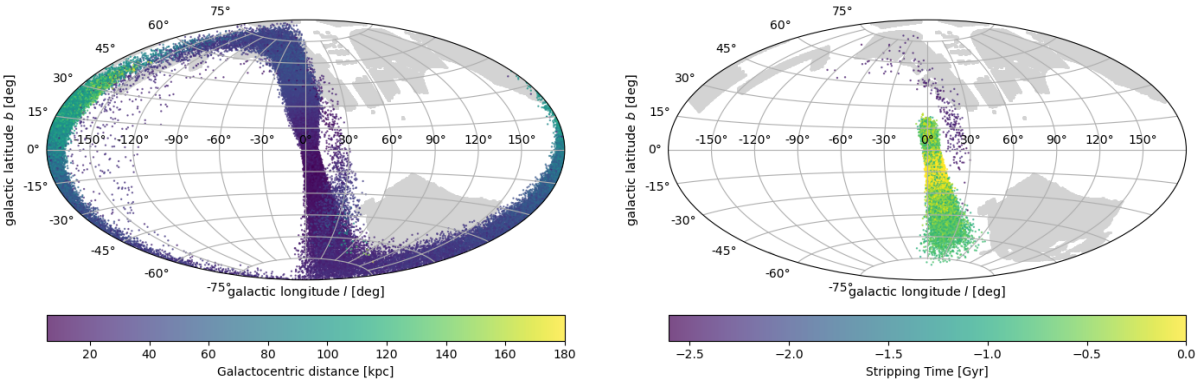

Figure 5: In the left panel, we show the Sagittarius stream overlayed on the footprint of our catalogue in grey, plotted in galactic coordinates and colour-coded by galactocentric distance. In the right panel, we show part of the stream reaching the galactocentric distances below 20 kpc, colour-coded by stripping time. Our sample lacks most of the Sagittarius galaxy, however, some stars still do trace the catalogue's footprint. The model stars belonging to the stream are taken from a simulation of the Sagittarius stream in the Milky Way and LMC potential by Vasiliev et al. (2021).

As the decomposition function takes absolute magnitude instead of luminosity, we compute it using $M_V = -2.5 \times \log_{10}\left(\frac{L}{L_\odot}\right) + M_{V\odot} = -17.43$ where we adopt $M_{V\odot} = 4.81$ from Willmer (2018) with 4% error. We find the corresponding error of the absolute magnitude of the halo using the method of partial derivatives (Blijleven, 2023): $\Delta M_V = \sqrt{(-2.5 \times \frac{\Delta L}{L \times \ln 10})^2 + (\Delta M_{V\odot})^2} = 0.30$. Furthermore, we tested the impact of an additional parameter `npar` which assigns the number of luminosity bins. We find that changing the parameter to a value different from the automatically assigned one changes the result significantly, so we continue with 1 mag-sized bins, which produce results consistent with the Deason et al. (2023) results (we show a comparison of these results for a dwarf galaxy in 3.2.1). Additionally, we tested the impact of different versions of imported packages on the results and found that they significantly differ in most cases, therefore we chose to adopt the ones which produce results that most closely resemble those of Deason et al. (2023) (we extend the discussion of this topic in the Appendix). Lastly, we looked into the parameter `nlive` which assigns the number of live points used for nested sampling and impacts the accuracy, but also the running time of the code. We used the 10000 live points, which was also suggested in the model of Deason et al. (2023). This way the model is able to explore the parameter space while still converging to an accurate result. The downside of using this many points, however, is that when applied to a sample of the size of ours, the runtime of the code dramatically increases (Speagle, 2020). Therefore, in order to combat this issue, we use multiple Virgo, Hydra and Norma machines in order to run the simulation for each of the 33 regions described above simultaneously. The `dynesty` package uses the Python `multiprocessing` module which employs data parallelism in order to run the code using multiple processors at once (Python Software Foundation, 2022). Therefore, running the regions on different machines improves the code's efficiency as each simulation is allocated a larger amount of processors than what it would have been if all regions were run on a single machine at the same time. It should be acknowledged that when applying the MDF decomposition code to the regions of the halo we make an assumption that stars belonging to each region represent the whole halo, which in reality is not the case. In other words, we model the galactic halo as if the metallicity distribution function of a given region mimics the one of the whole halo. Hence, we also use the total luminosity of the Milky

Way halo in order to set up each decomposition function. In addition to inspecting separate regions of the halo more closely, this also allows us to test how robust the inferences of the full halo are when one sees only a portion of it.

Upon further testing of the `nlive` parameter, we found that the MDF decomposition function is in fact quite robust to the change of the parameter for the tested range. It is visible from Figure 6 that the outcome of the decomposition model is relatively stable with respect to the change in the number of live points. However, it should be noted that the simulation with 1000 live points differs more from the one with 10000 points, compared to the simulation using 5000 points. We conclude that reducing the `nlive` to half its original value provides a good balance between the accuracy of the results and the runtime of the code. This finding allows us to model the complete halo catalogue in a reasonable period of time.

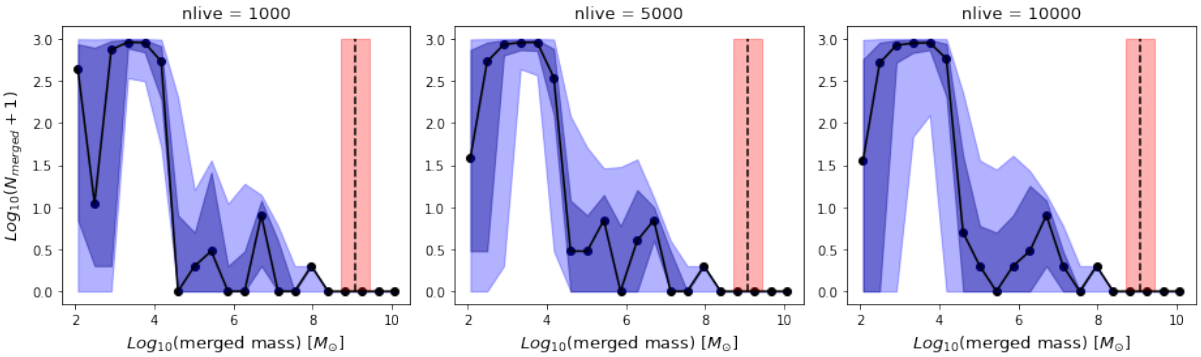

Figure 6: Robustness testing of `nlive` parameter for a region of stars (Region 1) with $0 <| b |< 30$ and $0 <| l |< 60$. The results of the MDF decomposition function are shown for three simulations with varying numbers of live points (from left to right): 1000, 5000 and 10000 points. The light purple regions show the 1-99 percentile, the darker purple regions show the 16-84 percentile, while the black line shows the median. The black dotted line represents the logarithm of the starting mass of the whole system, while the red area around it shows the error in this value.

Finally, in order to convert the luminosity output of the MDF function to the mass of accreted galaxies, we assume a stellar mass-to-light ratio of $M_*/L = 1.5$, which corresponds to the Kroupa initial mass function (Deason et al., 2019).

3 Results

In this section, we will present the results of the Gaussian mixture approach described in 2.2. Here we will divide the halo into three separate bins based on galactocentric distance as well as into three different intervals of heights from the galactic plane in order to explore the catalogue in more depth. Following this, we will present the results of the MDF decomposition for the 33 regions of the halo followed by a luminosity-spectrum of progenitors of the entire halo catalogue described in 2.1. We will then compare the results of our simulations to the results of Deason et al. (2023) who used a smaller and less homogeneous sample than the one used here. In addition to the results mentioned above, here we also include an exploratory plot of the metallicity of the catalogue's footprint in Figure 7. In order to closely examine how the metallicity of the halo changes as a function of position, we create $15° \times 15°$ bins of galactic latitude and longitude and compute the average [Fe/H] of each bin, the result of which can be seen in this figure. It is clear already that the metallicity of the Milky Way halo is not isotropic. We observe that the regions closer to the centre of the galaxy are noticeably more metal-rich.

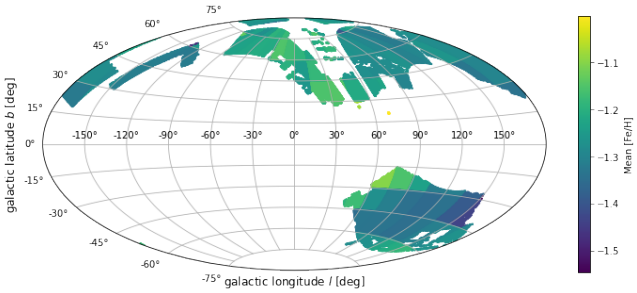

Figure 7: The catalogue divided into $15° \times 15°$ bins and colour-coded based on mean [Fe/H] of each bin. The vertical and horizontal axis show galactic latitude b and longitude l, respectively. The colour bar shows the mean metallicity.

In order to properly interpret the following results, it is crucial to understand the distance spanned by the catalogue. For this reason, in Figure 8 we show the footprint of our catalogue colour-coded for absolute height above the galactic plane | Z | in the left part of the figure as well as for galactocentric distance d in the right part of the figure.

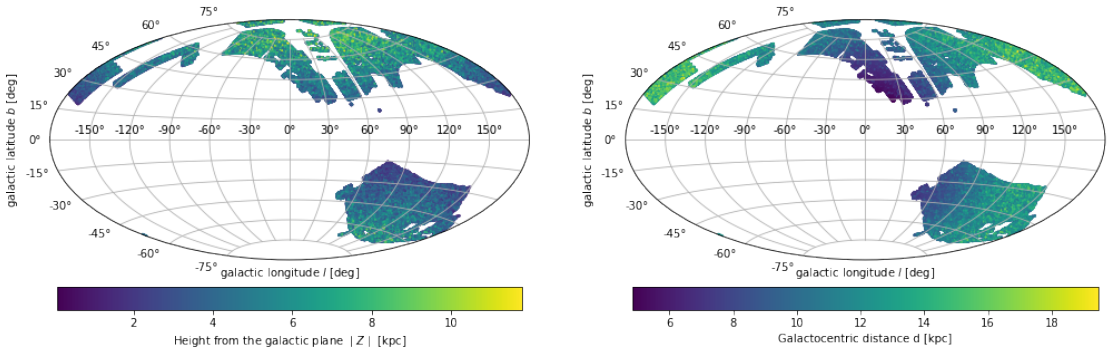

Figure 8: Footprint of the Pristine DR1 combined with the RPM catalogue in galactocentric coordinates. The left figure shows the absolute value of the height from the galactic plane Z for each star in the catalogue, while the right figure shows the galactocentric distance d.

3.1 Gaussian Mixture

In order to start the analysis of the Pristine DR1 and RPM catalogue, we first explore it by decomposing the MDF in an alternate way, as described in 2.2. We show the results of the Gaussian mixture method of investigating the halo in Figure 9 and Figure 10. Following this we present additional results derived using the same method in Figures 11 and 12.

3.1.1 Mean metallicity of stars

In Figure 9 we show the decomposition of the galactic halo for three ranges of height from the galactic plane (from top to bottom): $0 - 2.1$ kpc, $2.1 - 3.5$ kpc and $3.5 - 12$ kpc. Each of the ranges is created in such a way that all of them include about the same number of stars. They are divided further into the 33 regions of the sky shown in Figure 3. We then fit multiple Gaussian distributions to the overall MDF of each region using the `GaussianMixture` module. For most regions, this results in three fitted Gaussians that we interpret as kicked-up disc stars, accreted halo stars and the metal-poor tail as described in 2.2.

As was briefly mentioned in the Methods and Data Section, we refer to the most metal-rich component of the Gaussian mixture as a component of disc stars kicked up to halo-like orbits by a past merger event. Here we describe this conclusion in more depth. Using a large Gaia DR2 sample supported by additional spectroscopic information, Belokurov et al. (2020) find a predominantly old population of stars on highly eccentric orbits in the Solar Neighbourhood. However, they note that they are not as old as the last major merger event (GES), hence they conclude that these stars were born in the disc of the Milky Way but were kicked up to halo-like orbits as a result of the GES merger about 10 Gyr ago (Helmi et al., 2018) and name this component the *Splash*. They notice that this population is best visible in the $-0.7 < [\mathrm{Fe/H}] < -0.2$ range but believe that the component includes more metal-poor stars too. In Figure 4 we show that the most metal-rich component or our halo sample has a mean $[\mathrm{Fe/H}] = -0.67$, so it is likely that it represents the *Splash* stars as it encompasses the $-0.7 < [\mathrm{Fe/H}] < -0.2$ range, but also reaches lower metallicities, that are hypothesised to belong to this in-situ population as well.

We plot the mean metallicity of each Gaussian component for each region in the figure below. The columns of the figure along with their colour bars represent each of the halo components while the rows correspond to the height ranges. The vertical and horizontal axes show the galactic latitude b and longitude l, respectively. Despite our efforts of dividing the 3 distance bins into equal numbers of stars, some of the 33 regions of the footprint still lack the appropriate number of stars to achieve a proper Gaussian fit to the data. Therefore, some regions are excluded from the plots in order to avoid the statistics of small numbers. These regions are shown in light grey colour.

It is visible from the figure that the MDF of the halo indeed changes with varying heights from the galactic plane. The first column of Figure 9 shows that the kicked-up disc (*Splash*) stars increase in metallicity as we move further from the galactic plane. On the contrary, we see that the average metallicity of accreted halo stars and the metal-poor tail decreases further from the plane. Additionally, we notice from the second and third panels that at 2.1 kpc $<|$ Z $|<$ 3.5 kpc there is a significant difference between the northern and southern halo as the northern one is more metal-rich. We emphasise that the catalogue probes different on-sky footprints of the southern and northern halo, hence, we should not overinterpret these results.

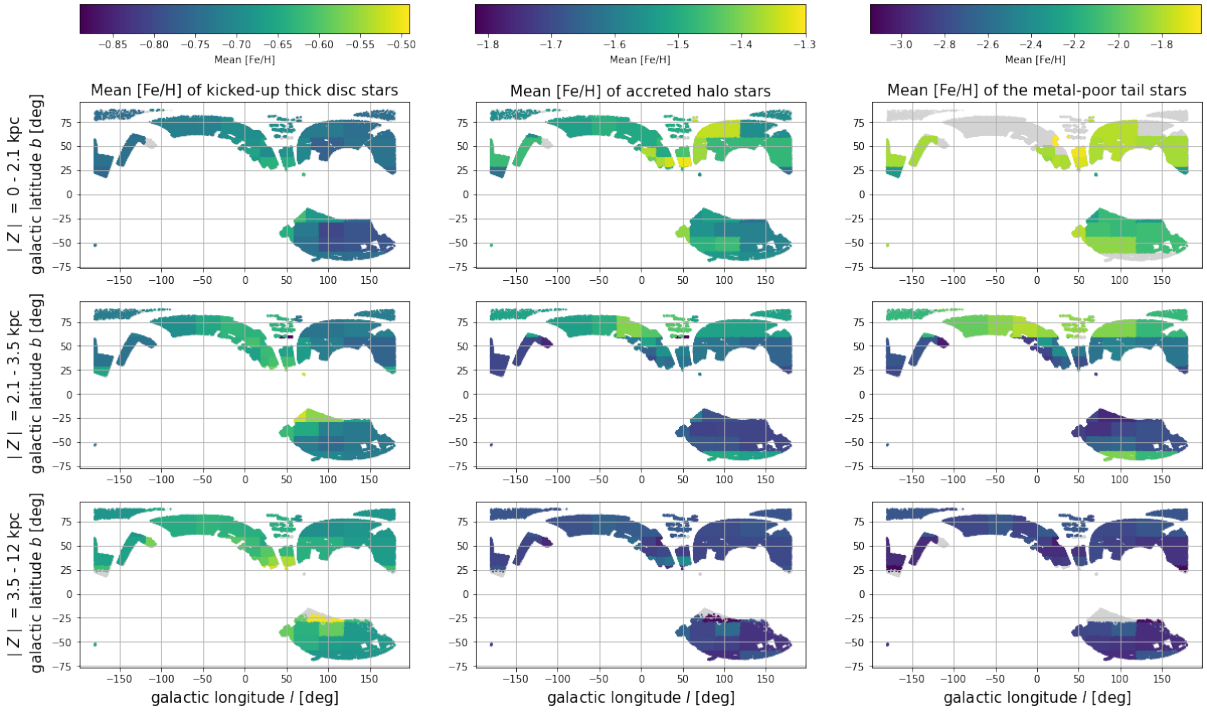

Figure 9: Decomposition of the galactic halo based on a Gaussian mixture of the MDF for three ranges of height from the galactic plane | Z |. The rows of the figure represent the following ranges (from top to bottom): $0 - 2.1$ kpc, $2.1 - 3.5$ kpc and $3.5 - 12$ kpc. The three regions were divided in such a way that each of them have about the same number of stars (100 000). Additionally, each distance interval is divided into 33 regions shown in Figure 3. Each column of the figure represents a different component of halo stars along with a colour bar showing the mean metallicity of each component of the halo. The columns are described as follows (from left to right): the first column represents the most metal-rich component of the halo, likely the kicked-up disc stars; the second column shows a more metal-poor component corresponding to accreted halo stars; lastly, the metal-poor tail of the halo is shown. It should be noted that the `GaussianMixture` module described in 2.2 could not properly fit all three components of the halo for all 33 regions. Hence, these regions are missing from the plots and are represented by light grey areas.

In Figure 10 we show results similar to those in Figure 9 with the distinction that here we use the following three galactocentric distance ranges (from top to bottom): $4 - 7.5$ kpc, $7.5 - 9$ kpc and $9 - 20$ kpc. Again, the ranges were picked such that they all have a comparative number of stars. From the first column, it is visible that mean metallicity decreases as we move further away from the galactic centre. Here we notice that the kicked-up thick disc component is especially metal-rich along a certain range of galactic longitudes ($-50° < l < 50°$), this is particularly the case for the distance bin furthest from the galactic centre ($9 - 20$ kpc). This finding indicates that a specific metal-rich component was displaced by the GES merger on these longitudes. Alternatively, it signifies the presence of a massive Milky Way progenitor, likely the Sagittarius dwarf galaxy, that distributed its stars perpendicular to the plane of the galaxy. We discuss this possibility further in 4.2.

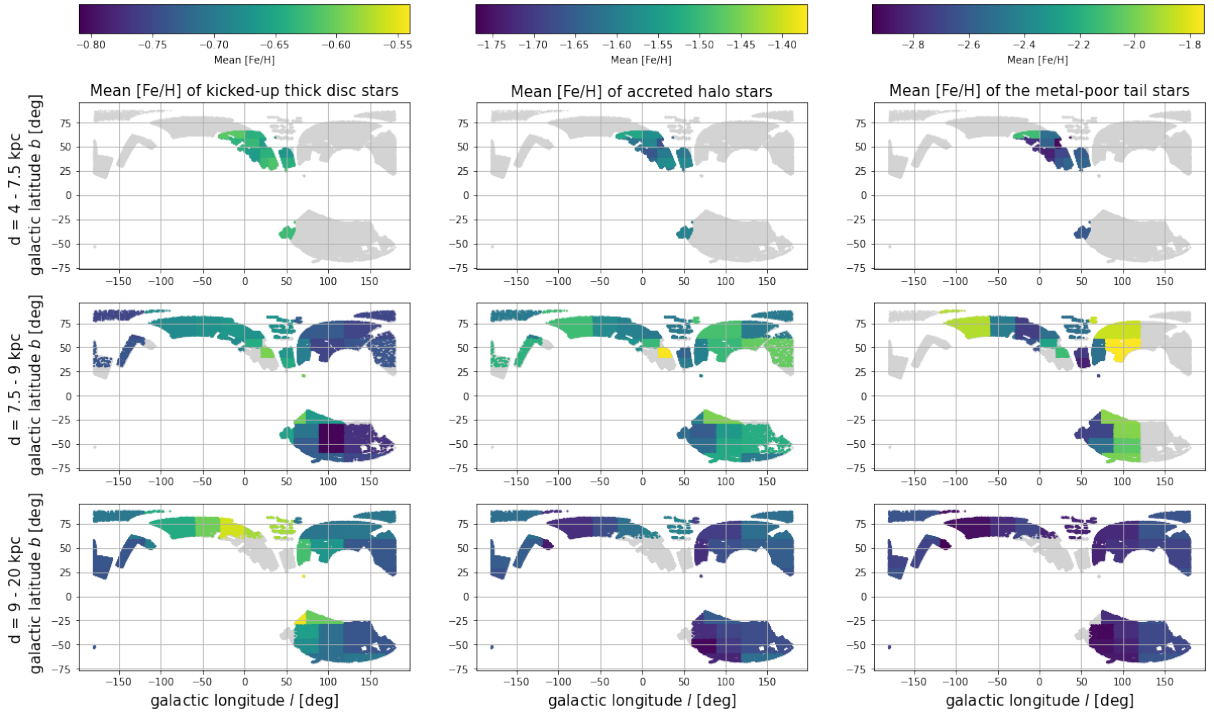

Figure 10: This Figure is analogous to Figure 9. Instead of three | Z | ranges, it shows three different galactocentric distance ranges chosen such that they have about an equal amount of stars in each. The ranges are taken as follows (from top to bottom): $4 - 7.5$ kpc, $7.5 - 9$ kpc and $9 - 20$ kpc. The three columns and corresponding colour bars of the figure can be described in the same way as for Figure 9. As a result of three different galactocentric distance intervals, some regions could not be decomposed into multiple Gaussians as they had only a few stars or none at all. These regions, along with some others that lack enough stars, are shown in light grey.

3.1.2 Fraction of stars

In addition to inspecting the mean [Fe/H], we take the analysis further by investigating the fraction of stars belonging to each component of the halo at different galactocentric distance ranges and heights of the galactic plane. Here we show the fractions of stars belonging to the three components of the halo defined in 2.2 for three distance intervals. The fractions in the figures are plotted such that the sum of fractions of stars in a given row for each region adds up to 1.

In Figure 11 we show the distribution of stars for the same three ranges of heights from the galactic plane | Z |. From these plots, it is visible that the largest component of the thick disc and metal-poor tail stars reside close to the galactic plane. While this is expected for the kicked-up disc stars as they come from the disc anyway, a larger fraction of metal-poor stars close to the plane is not as likely. Additionally, we see that a significant part of the footprint is missing from the metal-poor plot in the first row, hence we attribute this unexpected finding to the statistics of small numbers. We also notice an outlier region located around $b = 50°$ and $l = -110°$ in the third distance bin. From the third plot in the third column, we see that data for this region is missing, therefore, we conclude that this area could not be properly fitted and discard it from our analysis. Lastly, we find that the second panel of the third column shows that regions around $b = 75°$ include a larger percentage of metal-poor stars compared to their surroundings at the

same range of heights from the galactic plane.

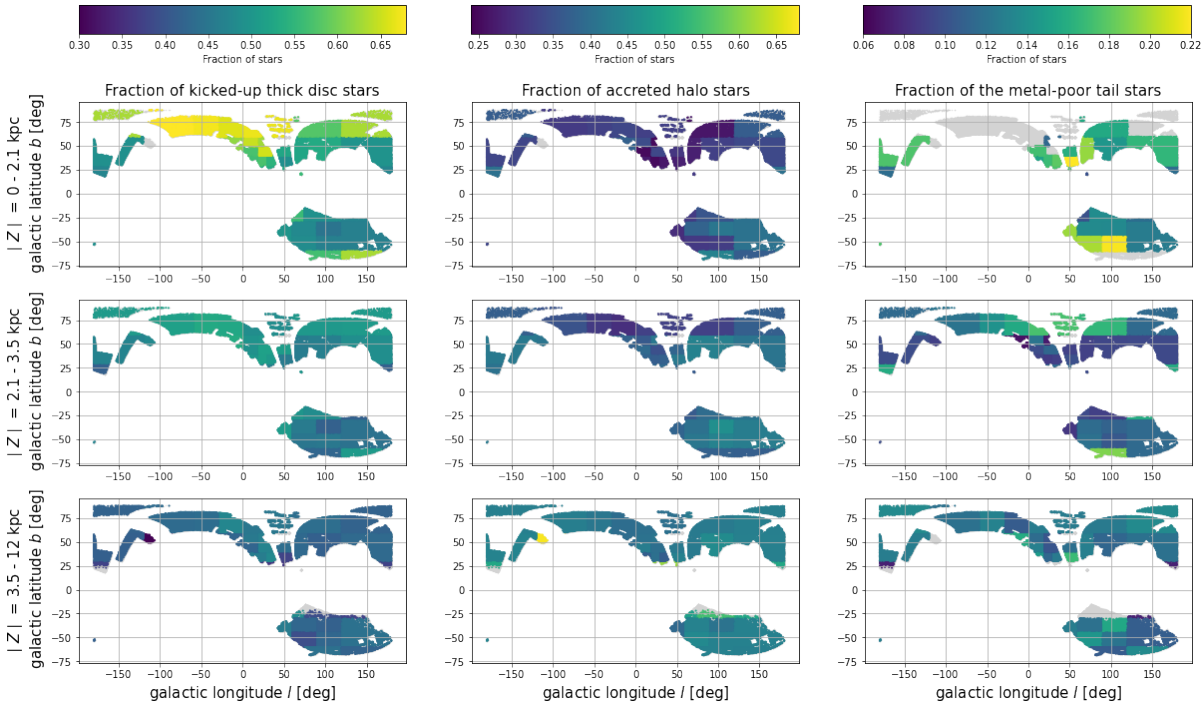

Figure 11: Decomposition of the halo based on a fraction of stars belonging to each component of the halo. Three ranges of height from the galactic plane | Z | are shown (from top to bottom): $0-2.1$ kpc, $2.1-3.5$ kpc and $3.5-12$ kpc. This figure is complementary to Figure 9 as instead of metallicity, the colour bar shows the fraction of stars in the regions shown in the figure. The grey regions, axes, columns and rows are the same as in Figure 9.

Figure 12 shows the results of the `GaussianMixture` module for three galactocentric distance ranges. The colour bar indicates the fraction of stars belonging to each component of the halo for 33 regions of the catalogue's footprint. As for Figure 11, the fractions are shown such that the sum of fractions along each row for a given region adds up to 1. The outlier region in the second row centred around $b = -50°$ and $l = 140°$ is excluded from our analysis as we notice that this region could not achieve a proper fit of three Gaussian components, but only two due to small number statistics. As the fitted components are not independent of each other but overlap, it is likely that the entire region was incorrectly fitted. It is evident from the figure that the largest percentage of kicked-up disc stars is visible in the $7.5-9$ kpc distance range, more specifically in the northern galactic halo and around $100° <| l |< 175°$. The second column of the figure shows the largest fraction of accreted halo stars furthest away from the galactic centre, in the $9-20$ kpc distance range. Finally, we see that the fraction of stars in the metal-poor component of the halo varies at all distance ranges, but it is especially large around $| l |= 100°$ in the $7.5-9$ kpc distance range.

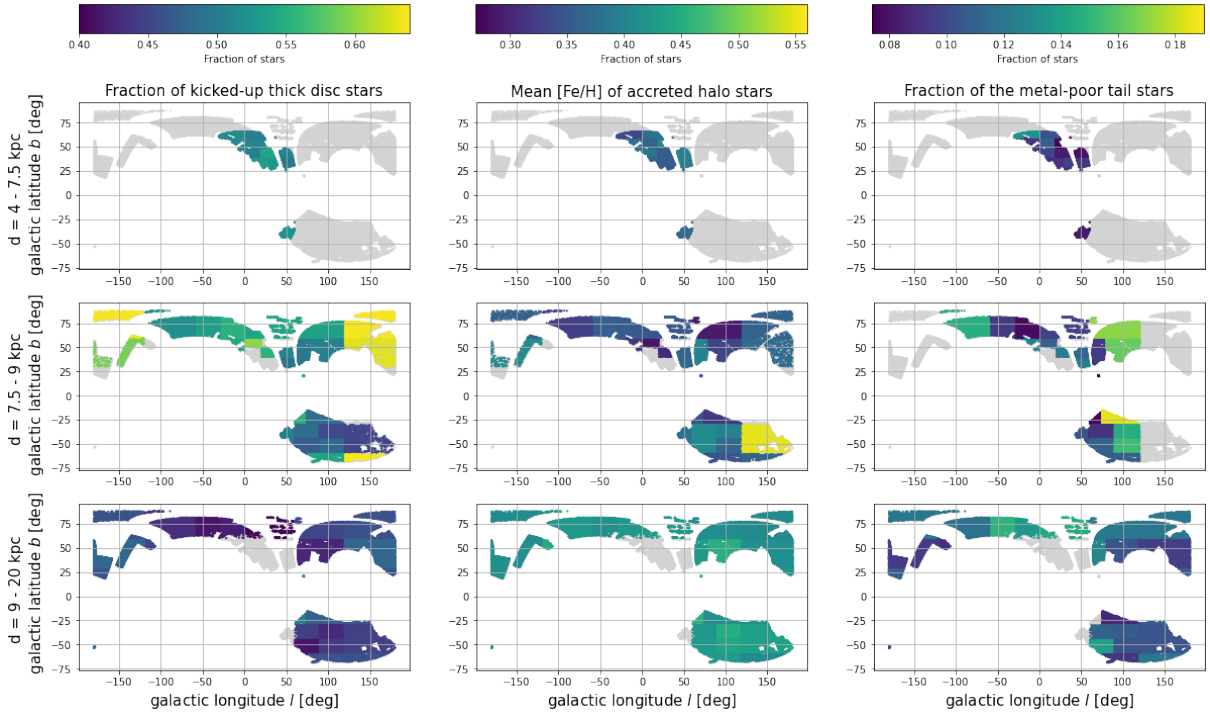

Figure 12: This figure is analogous to Figure 11 with the exception that it shows the fractions of stars based on three galactocentric distance ranges as opposed to height from the galactic plane. It shows three distance ranges (from top to bottom): $4 - 7.5$ kpc, $7.5 - 9$ kpc and $9 - 20$ kpc; and is complementary to Figure 10.

3.2 MDF decomposition

We will begin this subsection by presenting the result of the MDF decomposition of Fornax, a dwarf galaxy of the Milky Way in order to compare the result to that of Deason et al. (2023) as a sanity check. We will then present the results of the MDF decomposition for the 33 separate regions of the halo, followed by the results made with the entire halo sample and compare it to previous results from Deason et al. (2023).

3.2.1 Fornax

In Figure 13 we show the luminosity-spectrum of Fornax, a classical dwarf galaxy of the Milky Way. In the left panel we show our result and compare it to the result of Deason et al. (2023) in the right panel. This result serves as a test to ensure that our MDF decomposition module works properly and that the results agree with the authors'. For the MDF decomposition of this satellite, we use the same input as Deason et al. (2023): a sample of stars from Kirby et al. (2011) along with starting luminosity from McConnachie (2012) and the same number of luminosity bins that was automatically assigned; hence, we expect a very similar result to theirs. We find that the results are very similar. Hence, we continue our approach and apply it to our Milky Way halo catalogue using the automatically assigned number of luminosity bins.

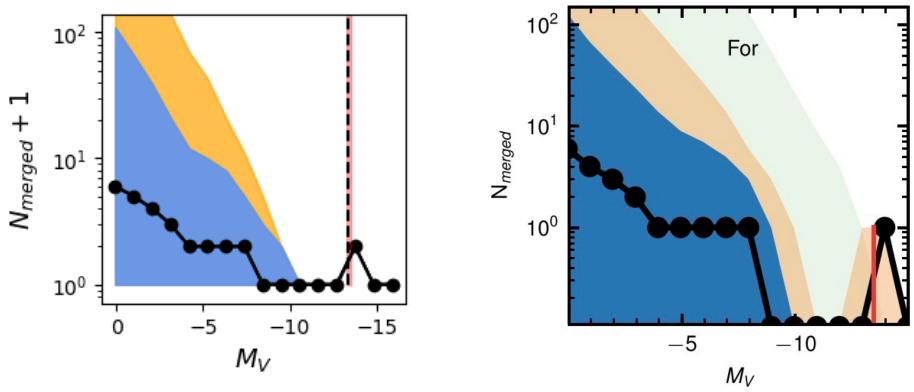

Figure 13: MDF decomposition of the Fornax dwarf galaxy. The left panel shows our result while the right panel shows Figure 2 from Deason et al. (2023) adapted to only show the result for Fornax. The horizontal axes show absolute magnitude while the vertical axes show the number of merged galaxies (the left plot is offset by 1 for plotting reasons). The yellow/orange regions show the 1-99 percentile and the blue regions show the 16-84 percentile. The black line is the median. The dotted black line and surrounding red area in the left panel show the starting luminosity of the dwarf galaxy and its error. In the right panel, the starting luminosity is shown by the red line.

3.2.2 33 regions of the halo

In Figure 14 we show the results of 33 simulations for 33 regions of the Pristine footprint. As previously stated, here we model the halo under the assumption that the modelled region of stars represents the whole stellar halo. The vertical axis of each plot shows the logarithm of the number of merged galaxies offset by 1 for plotting reasons. The horizontal axis shows the logarithm of the mass of merged galaxies. The lighter purple region shows the 1-99 percentile while the darker purple region shows the 16-84 percentile. The black line shows the median while the dotted black line and the surrounding red area represent the starting mass of the halo used for the simulations calculated using a stellar mass-to-light ratio of $M_*/L = 1.5$ and the luminosity stated in 2.3.1, along with its error.

This figure clearly shows the difference between the decompositions of MDFs amongst the regions. While most regions favour galaxies of small masses over more massive ones, regions from `5_c_2` to `8_c` with the exception of `6_c` show a preference for galaxies with masses of the order $10^4 - 10^6 M_\odot$. From this finding, it is clear that the halo is anisotropic and that it likely endured various mergers that are not fully mixed. As a consequence of the MZR, we can conclude that these regions are more metal-rich than the rest of the halo. Evidently, there is a difference in the chemical composition of the halo based on varying galactic latitude and longitude.

It should be noted that the mass-spectra of all the regions show a progenitor with a mass around $10^{7.5} M_\odot - 10^8 M_\odot$ indicating a likely merger with a massive galaxy sometime in the Milky Way history. Additionally, simulations of some regions show more convergence than others. This can likely be explained by a relatively small number of stars which produces a larger uncertainty, thereby causing the results to diverge at times. Alternatively, a wide spread of metallicities could result in a case in which the MDF decomposition model needs to more extensively explore the parameter space in order to converge. As a result, the model could not converge to a result with the given number of live points.

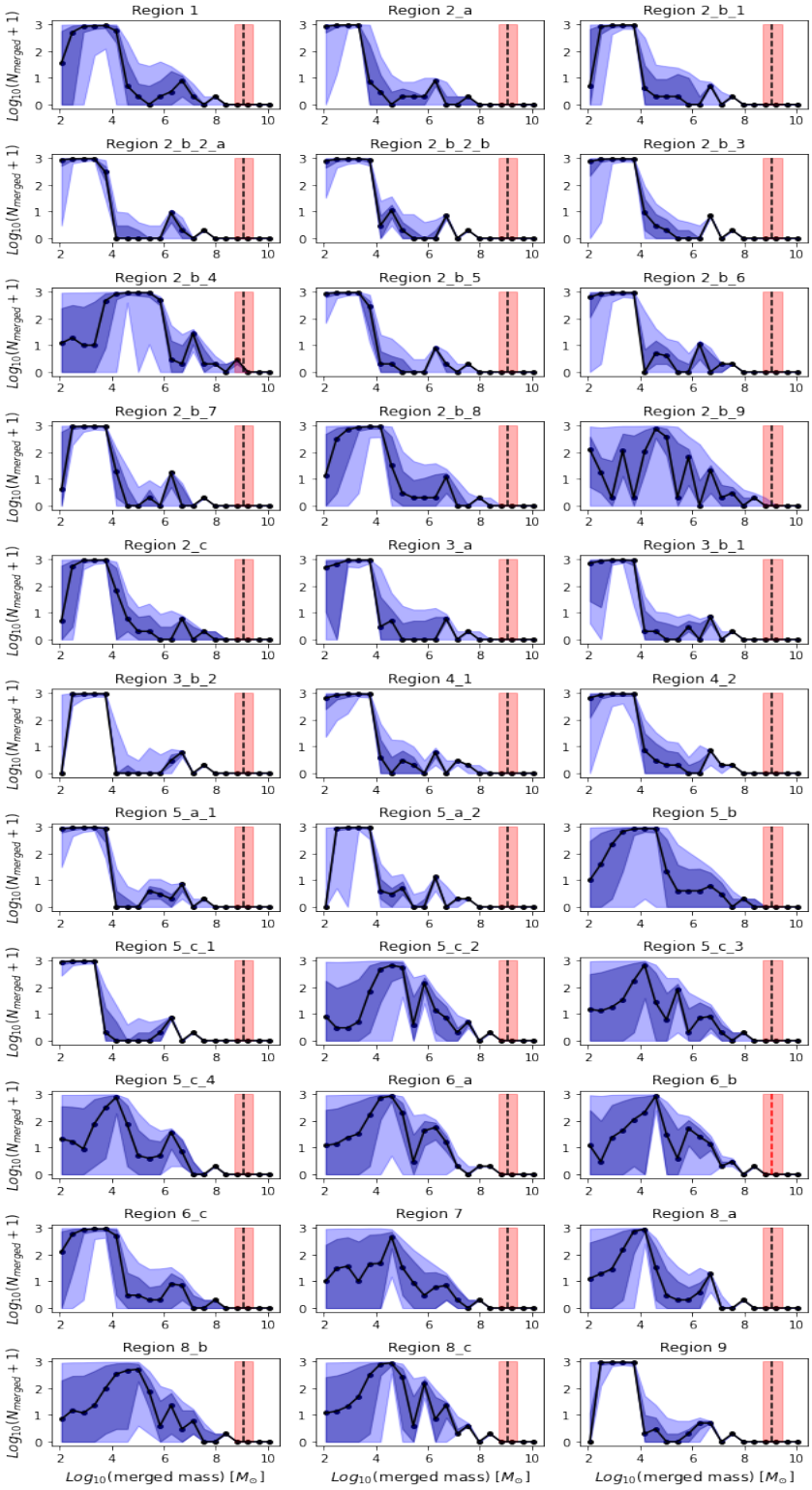

Figure 14: MDF decomposition for the entire halo catalogue divided into 33 separate regions based on galactic latitude and longitude. The y-axis of each plot represents the logarithm of the number of accreted galaxies offset by 1 for plotting reasons. The x-axis shows the corresponding logarithm of mass of the merged galaxies. The lighter purple regions show the 1-99 percentile, the darker purple regions show the 16-84 percentile, while the black line shows the median. The black dotted line and the red area around it show the initial estimate of the mass of the halo and its error, respectively.

3.2.3 Complete halo catalogue

Figure 15 shows the results of the MDF decomposition for the complete halo sample compared to the results from Deason et al. (2023). The horizontal axes of the plots show the absolute magnitude of the merged galaxies. The vertical axes of the left plots show the number of merged galaxies, while the vertical axes of the plots on the right show the cumulative number of merged galaxies. The dotted black lines and the shaded red area show the starting absolute magnitude of the halo and its error, respectively.

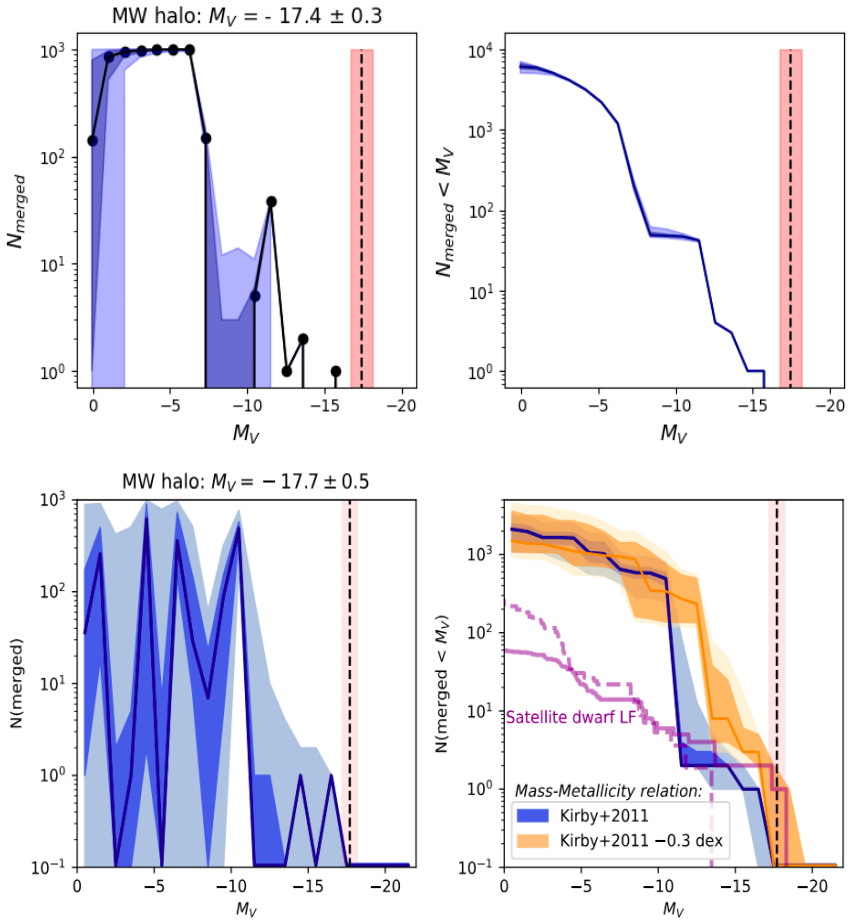

Figure 15: Comparison of results to Deason et al. (2023). The first row shows the results of the MDF decomposition function made using the Pristine DR1 and RPM catalogue described in Section 2 containing 294,015 stars. The second row shows a figure adapted from Deason et al. (2023) showcasing their results made with a catalogue of 21,813 stars. The plots on the left show a differential number of merged galaxies. The y-axis represents the number of merged galaxies, while the x-axis shows the absolute magnitude of the merged galaxies. The plots on the right side have the same x-axis, while the y-axis shows the number of merged galaxies smaller than a certain absolute magnitude, hence it shows a cumulative number of galaxies. The right figure from Deason et al. (2023) also shows the cumulative result of an alternative MZR that includes a −0.3 dex offset in orange and a satellite dwarf luminosity function in purple. In all figures, the black dotted line shows the starting absolute magnitude of the galaxy while the red area is the error in this value, while the different coloured regions are described in the same way as in Figure 14.

There are a number of important differences between the top and bottom rows of this figure. Firstly, the starting luminosity of the halo used in our simulation and the work of Deason et al. (2023) differs in value as well as precision. For their analysis, Deason et al. (2023) use a value of $M_V = -17.7 \pm 0.5$ while we adopt a value of $M_V = -17.4 \pm 0.3$ from Deason et al. (2019). Secondly, the first row of figures shows greater convergence compared to the second row. The top left plot of Figure 15 shows some error margins but seems to converge around $M_V = -5$ and after $M_V = -11$. This cannot be said for the bottom left plot. Consequently, the uncertainty margins follow the same trends for the cumulative plots too. This is likely due to the fact that our simulation uses over 10 times as many stars as the Deason et al. (2023) one. Finally, the most notable difference is the result itself. While the results of Deason et al. (2023) show a large amount of variation, our results seem to favour lower mass galaxies with $M_V < 7$. However, there does seem to be a similar peak around $M_V = -11$. While the amplitude of the peak estimated by our simulation is not as large, this could potentially indicate a significant amount of merger galaxies of said luminosity.

Furthermore, both cumulative plots show a similar shape, although our simulation predicts about 10 thousand mergers in the history of the Milky Way while this number is about a magnitude lower for the results of Deason et al. (2023). We notice a similarity between the steep drop of the graph around $M_V = -10$ in the lower right panel and around $M_V = -7.5$ in the top right panel. These findings suggest that our simulation favours less-massive galaxies, but still predicts similar trends as do the results by Deason et al. (2023). This can also point towards the difference in the sample of the halo used in both the simulations and imply that the Pristine DR1 and RPM halo catalogue includes more metal-poor stars than the combined spectroscopic sample used by Deason et al. (2023). We also note that since simulations based on our catalogue tend to estimate a larger number of faint galaxies, it is logical that the number of mergers will then be higher, as the total luminosity of the halo is modelled to add up to $M_V = -17.4 \pm 0.3$, or to $M_V = -17.7 \pm 0.5$ in the case of the lower part of the figure.

From the surviving dwarf satellite luminosity function (observed function by Nadler et al. 2020 and completeness-corrected function excluding the Sagittarius and Large and Small Magellanic Clouds by Drlica-Wagner et al. 2020) shown in the bottom right panel of Figure 15 we see that the number of dwarf galaxies estimated both by our results and those of Deason et al. (2023) at the fainter end of the luminosity spectrum is much higher than what the observational findings show. As noted by Deason et al. (2023), this discrepancy can be described by the MDF decomposition module overestimating the number of faint galaxies due to the assumption of a Gaussian MDF.

As one of the scientific goals of this work is to estimate the mass-spectrum down to the smallest galaxies that merged with our own, we will present the results as a function of solar mass from here on. In Figure 16 we show the mass-spectrum of the complete halo catalogue, offset by 1 for plotting reasons. From this figure, it can once again be inferred that less massive galaxies are highly favoured over massive ones. We find that there are 6027 galaxies with masses between $10^2 - 10^5$ $M_\odot$ and 46 galaxies between $10^6 - 10^8$ $M_\odot$. Finally, we find only one merger galaxy with mass round $2.5 \cdot 10^8$ $M_\odot$. This agrees with Deason et al. (2023) who find only one merger galaxy of a similar mass when using the Kirby et al. (2013) MZR (eq. 1). We find no mergers more massive than this one. For a more detailed discussion of the results, we refer to Subsection 4.3.

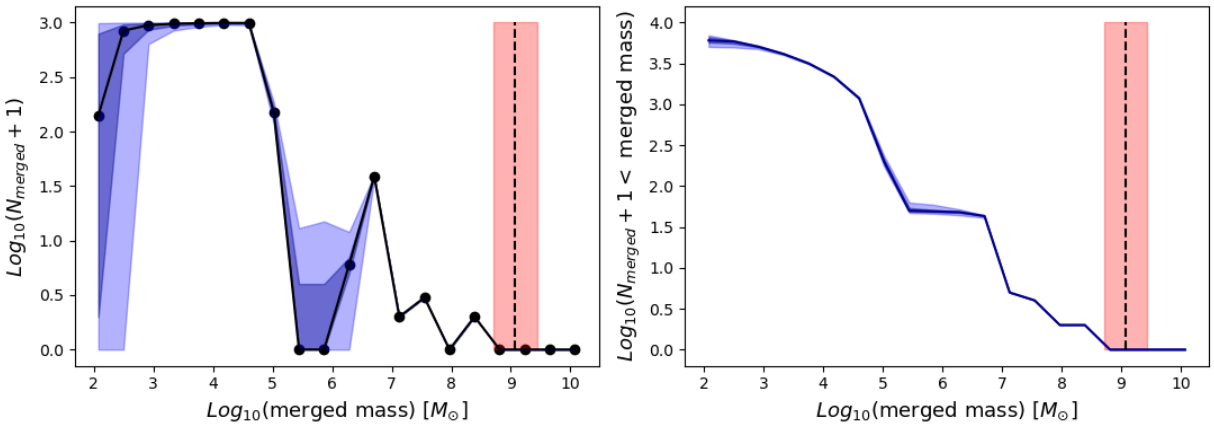

Figure 16: Number of accreted galaxies in the halo based on a sample of 294,015 stars and their metallicities. The left panel of the figure shows the differential number of accreted galaxies while the right panel shows the cumulative number. The horizontal axes of the plots show the logarithm of mass of the merged galaxies. The vertical axis of the left plot represents the logarithm of the number of accreted galaxies offset by 1. On the right, the vertical axis shows the logarithm of the number of merged galaxies (offset by one) smaller than a given mass. The lighter purple region shows the 1-99 percentile, the darker purple region shows the 16-84 percentile, while the black line shows the median. The black dotted line and the shaded red area represent the starting mass of the halo used for the MDF decomposition function and its error, respectively. It is clear that the simulation predicts more low-mass progenitors than massive ones.

4 Discussion

In this section, we will discuss the implications of the above-shown results and compare them to literature as well as mention their limitations and future areas of improvement. We start by discussing the catalogue of stars, followed by the discussion of the Gaussian mixture exploration of data. Next, we discuss the luminosity- and mass-spectra created using the MDF decomposition module as well as the compatibility of our catalogue with the module. Finally, we create an additional subset of stars and discuss its results and implications.

4.1 The Catalogue

In order to start our analysis of the galactic halo of the Milky Way, we first needed to find a homogeneous sample of halo stars with high-quality metallicities. We used a combined catalogue of the Pristine photometric survey (Martin et al., 2023) and the RPM catalogue (Viswanathan et al., 2023) described in more detail in 2.1. As both of these data sets have their own assumptions, their impact on our results will be discussed here.

Firstly, we will discuss the possible ways that caveats of the Pristine survey could affect the results. The most notable of those stems from the inaccuracy of the metallicites close to the bound of the metallicity grid ($-4.0 < [\mathrm{Fe/H}] < 0.0$). Martin et al. (2023) warn that the photometric metallicities of stars with $[\mathrm{Fe/H}]_{\mathrm{phot}} > -1.0$ could be biased in unexpected ways as the survey is better suited for metal-poor stars. As a significant fraction of stars in our catalogue belong to this range, it is possible that the catalogue poorly represents the actual MDF of the halo for more metal-rich stars in it. In addition to this, the Pristine DR1 metallicites are accurate down to $[\mathrm{Fe/H}]_{\mathrm{phot}} > -3.5$. Consequently, the stars below this value could also produce inaccuracies in the results. Therefore, the results at either end of the mass-spectrum should be carefully interpreted as this is where we expect the possible metallicity inaccuracies to carry over, as a consequence of the MZR. A possible future improvement would require placing an additional cut of $-3.5 < [\mathrm{Fe/H}]_{\mathrm{phot}} < -1.0$ on the metallicities of the sample such that the possibly inaccurate and problematic areas of the Pristine DR1 are avoided, combined with careful testing of applying such limitations on the input catalogue on the results. Lastly, it should be noted that during our inspection of the catalogue, we noticed a curious overdensity of stars with metallicities $[\mathrm{Fe/H}]_{\mathrm{phot}} \approx -0.3$. It was concluded that this is likely an artefact of the way metallicities are derived in the survey and is a consequence of smoothing over a grid of metallicities. Hence, this overdensity could contribute to the overestimation of less massive progenitors.

Secondly, we discuss how the assumptions about the RPM sample could affect our results. A crucial step in the creation of the RPM catalogue is placing a tangential velocity cut that selects only those stars with $200\ \mathrm{km\ s^{-1}} < v_{\mathrm{tan}} < 800\ \mathrm{km\ s^{-1}}$. As disc stars have low tangential velocities, this cut would remove them, resulting in a clean sample of halo stars. However, this assumption can cause some inaccuracies. As Viswanathan et al. (2023) mention, this cut inevitably excludes halo stars that are moving in a similar plane as the Sun and have low tangential velocities. Under the assumption that the excluded halo stars are completely random in metallicity, the RPM catalogue should still be left with a representative selection of stars, as we see various metallicity effects with $|\ Z\ |$, and differences can be expected.

While it does reduce the size of the sample, the exclusion of some halo stars is not as problematic as the inclusion of stars belonging to the disc. This likely pollutes the result and overestimates the number of metal-rich stars in the galactic halo by misattributing them to the halo instead of

the disc. Therefore, one should be careful when interpreting the results of the MDF decomposition. Looking at Figure 7 and the right panel of Figure 8, we notice that the most metal-rich regions coincide with the regions closest to the galactic centre. Hence, a fraction of bulge stars with high tangential velocities may pollute this part of the catalogue and bias it towards higher metallicities.

4.2 Gaussian Mixture

We begin the analysis of our catalogue by decomposing its MDF into multiple Gaussian distributions using the `GaussianMixture` module further described in 2.2. Here we will discuss the implications of the above shown results and discuss the potential drawbacks of this approach.

4.2.1 Data limitations

Firstly, we discuss the potential drawbacks resulting from the division of the catalogue into three distance bins based on | Z | and d, which are further divided into multiple regions of the halo. One of the more noticeable drawbacks of this method is exactly this division into 33 regions as it resulted in the exclusion of some parts of the halo. In order to properly create a Gaussian decomposition of the MDF into three halo components of a given region, it needs to have the appropriate number of stars. In some cases, this was not achievable as the additional division into smaller regions resulted in too little of a star count to even fit a single Gaussian. We excluded these regions, but also acknowledge that this step reduces our sample size and limits the impact of our results. Additionally, for some regions, only two Gaussian functions were fitted, for which we concluded that they represent the kicked-up disc and accreted halo component as the corresponding histograms seemed to lack the metal-poor tail. Here we note that such a conclusion could be a mistake, as it is possible that the MDF of these regions is poorly represented by our catalogue and hence it inaccurately lacks a metal-poor component. Therefore, we warn against the misinterpretation of the results for the regions that lack all three components, especially for those regions that stand out among a given patch of sky. We also note that even in the cases when three Gaussians are fitted, it is not clear if they correspond to the same three components in all the regions of the halo catalogue or if the components are polluted by misattributed stars. As the Gaussains are not independent of one another, it could be the case that the shifting of one peak towards lower metallicities also shifts the results of the remaining two components. Hence, these results should not be overinterpreted.

Moreover, we recognise the limitation of using large distance ranges as they limit the possibility of more precisely quantifying the difference in chemical composition amongst the distance bins. This issue arises from the lack of stars at some distances from the galactic centre as well as heights from the galactic plane. While the Pristine survey has a relatively deep halo sample, by applying quality cuts we greatly thin out the catalogue. As a result, we resort to larger distance bins in an attempt to avoid small number statistics, which we encounter even with just three bins. Therefore, a future improvement in this aspect would be the inclusion of more sources with high-quality metallicities, once data permits this.

4.2.2 Discussion of results

The results of this method are shown in Figures 9 and 10 colour-coded for the mean metallicity of a given Gaussian component of the halo, and in Figures 11 and 12 colour-coded for the fraction of

stars in those components for both bins of galactocentric distances and heights from the galactic plane.

4.2.2.1 Height from the galactic plane ranges

By looking at the first column of Figure 9, we notice that the metallicity of the kicked-up disc component increases as a function of | Z |. This could point towards the conclusion that more metal-rich stars were kicked to outer halo orbits, therefore enriching the furthest distance bin (3.5 − 12 kpc). However, looking at Figure 11, we find a surprising result that the fraction of thick disc stars actually decreases as | Z | increases. This opposite trend and gradient in metallicity could potentially signify that the GES merger resulted in an anisotopic dispersion of *Splash* stars based on their metallicities, so more metal-rich stars were kicked up further in the halo. As we see no obvious reason for this case, we point towards an alternative solution. It is possible that there is a metal-rich component of halo stars at a higher distance of the galactic plane as a result of a previous massive merger.

As mentioned previously, we also notice that the second and third panels with 2.1 kpc $<$ | Z | $<$ 3.5 kpc range in Figure 9 show a significant difference between the northern and southern halo. This could point to a stream or a more massive merger galaxy in the Milky Way's history that brought in relatively "metal-rich" stars in the northern galactic hemisphere. Complementary to this, in Figure 11, we see that the second panel of the third row displays a larger fraction of stars in the northern hemisphere, further signalling that there is a possible over-density of stars, as a result of a progenitor galaxy. Based on the simulation of the Sagittarius dwarf galaxy in the potential of the Milky Way and the LMC in Figure 5, we see that an older wrap of the galaxy traces over the footprint of the northern hemisphere. As this component of the Sagittarius is stripped from the dwarf galaxy about 2.5 Gyr ago, it is possible that the simulation does not estimate their location with full certainty. Hence, there is a possibility that the difference in metallicity of the northern and southern halo in this figure is a result of this massive dwarf galaxy depositing its stars in the northern hemisphere.

4.2.2.2 Galactocentric distance ranges

We now turn our attention to Figures 10 and 12 which show the result of the Gaussian mixture method for three galactocentric distance bins. As mentioned earlier, we find that the most metal-rich component of the halo stars is particularly metal-rich in the $-50° < l < 50°$ range, especially in the $9 - 20$ kpc distance bin. Earlier we mentioned the possibility of this merger being the Sagittarius dwarf galaxy which distributed its stars perpendicular to the galactic plane. Looking at Figure 5, we find that there is a fraction of Sagittarius stars tracing a similar area as the more metal-rich regions of the kicked-up disc component in the $9 - 20$ kpc distance bin in Figure 10. Looking at the right panel of Figure 5, we see that these stars span a $10 - 20$ kpc distance range. It is therefore likely that we are capturing the Sagittarius stream in the $9 - 20$ kpc galactocentric distance bin. Moreover, from Figure 12 we see that this area includes a relatively small faction of stars. Therefore it is possible that the fraction of Sagittarius stars dominate the metallicity of these regions. While this is an exciting result, it also points towards an inconsistency in the Gaussian mixture method as it misattributed this accreted component of stars to the kicked-up disc component.

In addition to this, we find that the fraction of stars of the accreted halo component and the metal-poor tail are pretty varied. However, we do notice a correlation between the second panels

of the third column in the two figures. Here we see that the metallicity of stars around $\mid l \mid = 100°$ is higher compared to its surroundings and we also notice a higher fraction of stars in this region. From this, we infer that there is likely an overdensity of stars with [Fe/H] ≈ -2 in this region of the halo. Based on literature findings (Vivas et al. 2016, Balbinot and Helmi 2021, Perottoni et al. 2022), we believe that the overdensity of stars centred around $l = -100°$ and $b = 60°$ with mean [Fe/H] $= -1.9$ likely corresponds to the Virgo Overdensity.

Finally, we note that we cannot draw any conclusion based on similarities between | Z | and d ranges as stars in one | Z | bin are present in all d bins, and vice-versa.

4.3 MDF decomposition

In this subsection, we will discuss the assumptions of the MDF decomposition function as well as the results and their comparison to the literature, possible improvements and future work. Finally, as mentioned above, we will also include additional results based on a newly introduced subset of the catalogue.

4.3.1 MDF decomposition function

The assumptions of the MDF decomposition method itself should be discussed. The central assumption of this model is that the MDF of a galaxy can be represented as a mixture of MDFs of smaller galaxies. By inspecting the MDF of our halo catalogue in Figure 4, it is clear that the metallicity distribution of the galactic halo is indeed not a simple Gaussian, but a mixture of multiple. However, it is not evident if the expectation of MDFs of smaller galaxies being represented as simple Gaussian functions holds. This assumption breaks down in the event that one (or more) of the merger galaxies of the Milky Way experienced mergers in its past too. This would mean that its MDF is likely better represented by a mixture instead of a single Gaussian function. Moreover, Leaman (2012) shows that the MDFs of dwarf galaxies are clearly not perfect Gaussians as they have low-metallicity tails. The authors of the MDF decomposition warn that this assumption could result in overestimating the number of fainter accreted galaxies. Additionally, then warn that about $0.1 - 1\%$ of accreted halo stars actually come from globular clusters, hence we could be misinterpreting their origins.

Moreover, based on the results of 33 different regions in Figure 14, it is apparent that the decomposition function is sensitive to small differences in MDFs. We find that the panels in this figure show significant differences and different levels of convergence. Hence, we conclude that the method is not robust for small differences in the chemical composition and emphasise the importance of choosing a suitable sample when using this method.

4.3.2 Discussion of results

Here we will discuss the differences between our results and the literature, mainly focusing on the paper of Deason et al. (2023) and the results therein. Firstly, we will compare the dataset used by Deason et al. (2023) to the Pristine DR1 and RPM catalogue we use here. The most notable difference between the two is their size. The sample used by Deason et al. (2023) contains 21,813 stars, while our catalogue contains 294,015 stars. Not only is it more than 10 times larger, but the advantage of the Pristine DR1 and RPM catalogue also lies in the fact that it is a homogeneous sample where all the metallicities are measured and calculated in the same way. Due to the lack of a better sample at the time, Deason et al. (2023) settled on a combined sample of

multiple spectroscopic surveys. They cross-match sources from Gaia DR3 (Gaia Collaboration et al., 2023) to the following surveys: SDSS, The Radial Velocity Experiment (RAVE, Kunder et al. 2017), LAMOST, APOGEE and Galactic Archaeology with HERMES survey (GALAH, Buder et al. 2021). After applying quality cuts, they are left with a sample that contains the above-mentioned number of halo stars. The disadvantage of this sample is that it is susceptible to metallicity biases due to its inhomogeneity. Because the metallicities in these surveys are derived and measured using different selection functions, each of them may carry a bias or an offset to the metallicity measurements that are not corrected for when combining them. This is also pointed out by the authors themselves. Therefore, we conclude that it is precisely the number of stars and the (in)homogeneity of the catalogues that make the difference in the results.

While the MDF decomposition model should not be affected by the number of stars in a sample, it strongly depends on how representative it is for a given region. As mentioned previously, this is apparent in Figure 14 as we find that the mass-spectra significantly differ based on which region of the halo is modelled. As our sample contains a larger amount of stars, it is statistically a better representation of the MDF halo as a whole compared to the smaller sample of Deason et al. (2023). Due to a larger number of stars in our sample, the MDF code produces results with a smaller uncertainty margin. This describes why the results of the Deason et al. (2023) shown in the lower half of Figure 15 have a smaller degree of convergence compared to the results in the upper half of the figure. Furthermore, the results could partly diverge due to the use of different starting absolute magnitudes and their uncertainty in the setup of the simulations. Because Deason et al. (2023) use a larger error, we would expect their results to have wider uncertainty margins. As mentioned in 2.3.1, we use a value of $M_V = -17.4 \pm 0.3$, while Deason et al. (2023) opt for $M_V = -17.7 \pm 0.5$. However, the code has the freedom to go over the starting luminosity of the galaxy if the parameter `magpad` is set up in such a way. The hard-coded value of this parameter is 2.5, meaning that the MDF code is able to model the total luminosity of the galaxy that is 2.5 magnitudes smaller than the one initially given. We have not adjusted this value in our models, and as Deason et al. (2023) do not comment on it, we assume that they have not changed it either. Therefore, it is safe to assume that the simulations both had the same amount of freedom in this aspect. Hence, the slightly different starting luminosities are likely not the cause of diverging results.

Furthermore, we find that the number of luminosity bins used by the MDF simulation causes significant differences in the results. Deason et al. (2023) use 1 magnitude large luminosity bins which is also the automatic size assigned by the module itself. For them, this results in 22 bins. However, when we use the same-sized luminosity bins that are automatically assigned by the code, we end up with 20 bins. Additionally, we find that using any other number of bins significantly changes the results of our simulation (we once again refer to the Appendix for discussion of this topic), hence we hereby warn that the module is very sensitive to the change in the number of luminosity bins described by the `npar` parameter. As was described in 3.2.1, by first testing the simulation on Fornax, we find that using the automatically assigned number of bins yields results closest to the authors'. Hence, this is why we opted for 20 automatically assigned bins for our final results too. Finally, as Deason et al. (2023) do not comment on the value of the `nlive` parameter, we assume that they have not changed it from the hard-coded value of 10000. As we have shown in Figure 6, the difference between the use of `nlive` = 10000 and `nlive` = 5000 is not a significant one, therefore this parameter is likely not a contributor to the disparity of the results.

From Figure 15, we find 6032 progenitors with $M_V \gtrsim -10$, while Deason et al. (2023) find

about 400 progenitors of this luminosity. In total, we recover 6074 galaxies and find that our result is dominated by small progenitors, as only 47 progenitors fall between 10^6 $L_\odot$ to $10^{8.5}$ $L_\odot$. It is important to bear in mind the possible bias in this result. As mentioned previously, the assumption of a Gaussian MDF is likely to cause an overestimation of results at the fainter end as was demonstrated by the dwarf luminosity function in Figure 15 which clearly estimates a lower number of faint dwarf galaxies. We recover one massive progenitor with luminosity $\approx 10^{8.2}$ $L_\odot$ for the Kirby et al. (2013) MDF, which agrees with the findings of Deason et al. (2023). Using the stellar mass-to-light ratio of 1.5, we find the total mass of this accreted galaxy to be approximately $2.5 \cdot 10^8$ $M_\odot$. Interestingly, this value is close to recent estimates of the stellar mass of the GES merger (Naidu et al. 2021 and Lane et al. 2023). As mentioned previously, we also recover a progenitor of similar mass ($\sim 10^{7.5} - 10^8$ $M_\odot$) in all of the 33 region mass-spectra and conclude that they are likely pointing towards the same merger galaxy which disposed of its stars over the entire footprint of our catalogue. As authors of the MDF decomposition module find that the method is accurate up to 50 % for most luminosity bins, we conclude that the most massive progenitor we recover is likely the GES.

Lastly, based on the Kirby et al. (2013) MDF, we estimate the total luminosity of the Milky Way halo to be $(4.1 \pm 1.4) \cdot 10^8$ $L_\odot$ and following from this, we estimate the stellar mass of $(6.1 \pm 2.1) \cdot 10^8$ $M_\odot$. We notice that these estimations correspond to about 75 % of the value found by Deason et al. (2019) and are inside the uncertainty margins of their estimate. The lower estimate is likely a result of the distance range spanned by the catalogue ($4 - 20$ kpc from the galactic centre), while to determine the luminosity, Deason et al. (2019) use a selection of stars spanning a $5 - 100$ kpc distance range. Hence, it is clear that the RPM catalogue may be excluding stars brought in by galaxy mergers residing fully further out than 20 kpc in the halo. We conclude that the results are better understood as the total luminosity- and mass-spectrum of the dwarf galaxies whose pericentre is located inside $4 - 20$ kpc from the galactic centre. Therefore, we find that this region of the halo is composed of stars brought by about 6000 smaller dwarf galaxies with sizes comparable to Canes Venatici, Hercules and Ursa Major; about 50 more massive ones comparable to Sculptor, Fornax and WLM (McConnachie, 2012); and one massive galaxy, most similar to the GES. A future improvement in this area would involve using a sample of stars spanning a galactocentric distance range of up to 100 kpc. This approach would likely yield an estimate of halo luminosity more consistent with that of Deason et al. (2019) and would alter the mass-spectrum of the halo to better reflect its merger history.

4.3.2.1 Purely accreted halo subset

So far we have discussed the downside of the combined spectroscopic sample used by Deason et al. (2023) and its possible implications on the results of MDF decomposition, but we have yet to comment on the possible downsides of our catalogue. As described in subsection 2.2 about the exploration of the data set, by fitting a Gaussian mixture to the MDF of the halo catalogue we find an unusually metal-rich component that we consider to be a component of disc stars kicked up to highly eccentric halo-like orbits as a result of a past accretion event. i.e., the *Splash* (Belokurov et al., 2020). Moreover, using a chrono-chemo-dynamical analysis of main-sequence turnoff and subgiant stars, Nepal et al. (2024) find that there is a significant fraction of relatively metal-rich stars on highly eccentric near-halo or *Splash* orbits, with $-0.75 < [\mathrm{Fe/H}] < 0.0$. If this really is the case, we would then be falsely attributing these in-situ stars on halo-like orbits as being accreted onto the Milky Way by smaller mergers in the past. The inclusion of such metal-rich component could result in the MDF decomposition module overestimating the number of massive galaxies that merged with our own. For this reason, we create an additional

subset of the catalogue from which we statistically exclude the fraction of stars contributing to the metal-rich peak. Besides this, in Figure 1 of their paper, Deason et al. (2023) show that the expected input of the MDF decomposition module is very clearly a Gaussian MDF, which has asymmetric tails. As can be seen in Figure 4, the halo catalogue we use is more comparable to a double-peaked Gaussian, therefore we conclude that it is not a suitable shape for this method and could yield unreliable results.

In Figure 17 we show the MDF of the new selection of stars in purple compared to the overall MDF of the catalogue in blue. The exclusion of the kicked-up disc component reduced the catalogue to about half its original size, therefore it is expected that the results of the MDF decomposition of this subset will also differ from those shown in 3.2. Additionally, we notice that the shape of the MDF is now closer to a single-peaked Gaussian that the MDF decomposition module anticipates, so for this reason we expect the results of the simulation to be more accurate than those for the entire catalogue.

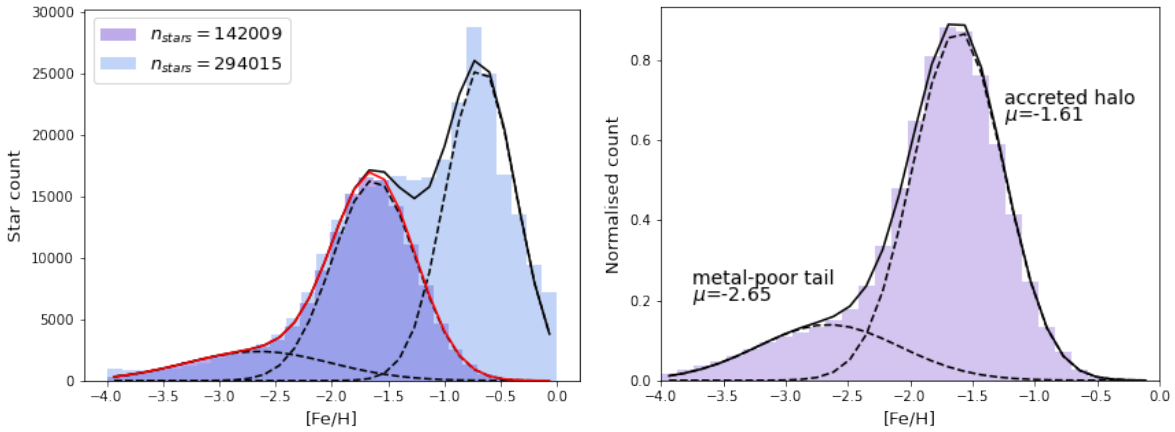

Figure 17: The left part of the figure shows the comparison of the MDFs of the complete halo catalogue and the subset of stars with the metal-rich Gaussian removed from the catalogue. The light blue histogram shows the MDF of the complete halo and includes 294,015 stars while the purple region shows a total of 142,009 stars. The horizontal and vertical axes of this plot show the metallicity and the star count in each bin on the histogram, respectively. The dotted lines correspond to the three Gaussians fitted by the `GaussianMixture` module, while the black line corresponds to the sum of the three. The red line shows the sum of the metal-poor tail and the accreted halo component and is the region of the MDF that we use to create the new subset of stars. On the right, we show a Gaussian decomposition of the new MDF where two Gaussians are fitted and represented by dotted lines. This plot is normalised, hence the vertical axis shows the normalised count of stars, while the horizontal axis still shows metallicity.

The difference between the catalogue and its new subset is also evident in Figure 18 which shows how the metallicity of the sample changes as a function of position in the galaxy. This figure is analogous to Figure 7 and was created in the same manner, but using the right panel of Figure 17 as input. As expected, the figure demonstrates that the metallicity of the reduced catalogue without the metal-rich *Splash* stars is more metal-poor for all regions of the halo compared to Figure 7. We find that the average metallicity of the entire catalogue reduces from [Fe/H] $= -1.24$ to [Fe/H] $= -1.83$. Interestingly, the mean metallicity does not vary significantly based on position, so we conclude that the chemical composition of the halo based on this sample is fairly isotropic.

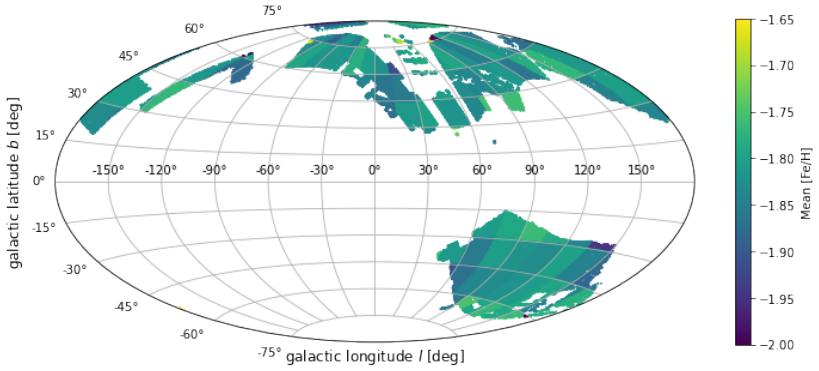

Figure 18: Subset of the catalogue excluding the metal-rich Gaussian divided into 15° × 15° bins and colour-coded based on mean [Fe/H] of each bin. The vertical and horizontal axis show galactic latitude b and longitude l, respectively. The colour bar shows the mean metallicity.

Finally, in Figure 19 (purple line) we show the mass-spectrum of the halo for merger galaxies whose pericentre is in $4 - 20$ kpc distance range for the subset of stars excluding the kicked-up disc stars. We note that the results of this subset were created using updated versions of some Python packages used by the MDF decomposition code, however, for reasons discussed in the Appendix, we find that the results are similar to those prior to the system update. Hence, we proceed disregarding this inconsistency.

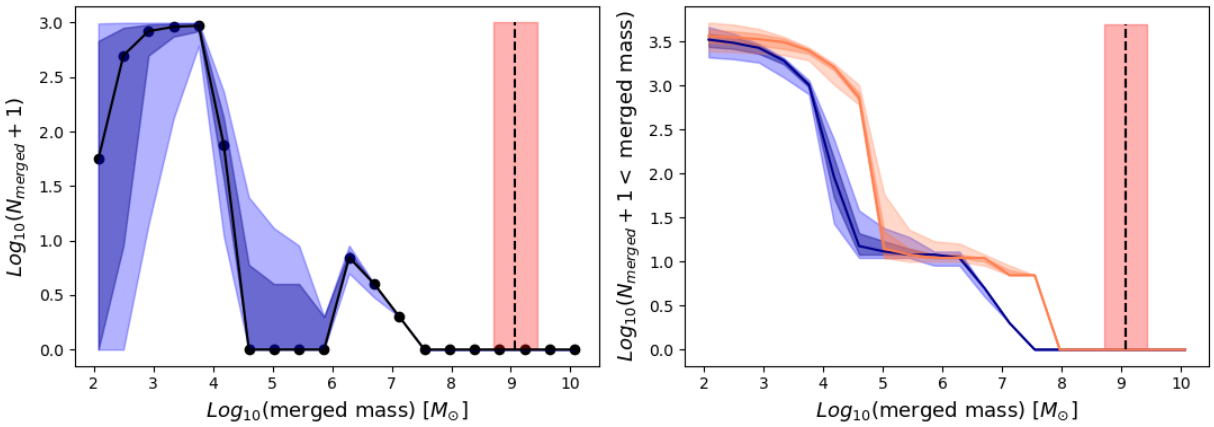

Figure 19: Mass-spectrum of the MDF decomposition for a subset of the halo catalogue excluding kicked-up in-situ disc stars. This figure is analogous to Figure 16 as it shows a differential and a cumulative number of merged galaxies but for a smaller subset of the catalogue (in purple). Additionally, another cumulative relation is plotted (in orange): the Kirby et al. (2013) MZR with a −0.3 dex offset, which was found to be more suitable for destroyed dwarf galaxies (Naidu et al., 2022).

It is clear that the results changed significantly compared to those in Figure 16. Firstly, we find that the number of progenitors with masses between 10^6 $M_\odot$ to $10^{8.5}$ $M_\odot$ significantly decreased from 47 galaxies to 10 galaxies. This is likely a consequence of the reduced fraction of metal-rich stars. Additionally, we observe that the number of less-massive galaxies with masses between 10^2 $M_\odot$ to 10^5 $M_\odot$ also reduces to 3313 progenitors. In total, this subset of the catalogue estimates about half as many progenitors as the complete halo catalogue. Moreover, we see that the

ratio of less-massive ones ($M < 10^5 M_\odot$) and massive galaxies ($M > 10^5 M_\odot$) differ significantly between the two sets of stars. While for the complete halo catalogue we find this ratio to be ~ 130, it reaches ~ 330 for the exclusively accreted component of the catalogue. This finding suggests that the reduced subset of stars highly favours less-massive galaxies over massive ones. This can likely be explained by the fact that the subset includes a significant fraction of metal-poor stars, which by virtue of the MZR, come from faint and small dwarf galaxies. Additionally, by comparing the cumulative plots in these figures, we find a steep decrease in the number of mergers around 10^4 $M_\odot$, compared to 10^5 $M_\odot$ in Figure 16, further signifying that the subset favours even smaller dwarf galaxies than our initial catalogue.

Lastly, we uncover 3319 galaxies with mass $\lesssim 10^6$ $M_\odot$ or $M_V \gtrsim -10$. It was previously noted that the non-Gaussianity of an MDF leads to the overestimation of faint galaxies. In Figure 17 we see that the shape of this subset of stars is similar to a Gaussian function with a more pronounced metal-poor tail, therefore overestimation of progenitors should not cause an issue here. While we do see a reduced number of faint galaxies compared to our first result, it is still significantly more than 400 galaxies estimated by Deason et al. (2023). Therefore, we can securely conclude that this increase in faint galaxies is a result of a catalogue that includes numerous stars with high-quality metallicities down to the extremely metal-poor end, as opposed to an estimation error. However, in the bottom right panel of Figure 15, we see that the surviving satellite dwarf luminosity still estimates a smaller number of dwarf galaxies compared to these results, hence, these results should still be interpreted with caution. Overall, we find that the region of the halo spanning the distance of $4 - 20$ kpc is composed of stars brought in by about 3000 galaxies with masses similar to Canes Venatici, Hercules and Ursa Major and only 10 more massive galaxies comparable to Sculptor, Fornax and WLM (McConnachie, 2012).

Furthermore, from this mass-spectrum, we estimate the mass of the accreted component of the halo. Once again, we emphasise that these results describe the component of stars which were accreted onto the Milky Way halo by galaxies whose pericentre is somewhere between 4 and 20 kpc from the galactic centre. We find that the mass of this accreted component in the Milky Way halo is $(5.0 \pm 1.7) \cdot 10^7$ $M_\odot$ and luminosity $(3.3 \pm 1.1) \cdot 10^7$ $L_\odot$, which is about two orders smaller than the starting luminosity we supplied to the model. While surprising at first, we realise that this reduction in luminosity and mass is a consequence of removing the most metal-rich stars from the MDF decomposition. It is important to emphasise that *Splash* stars, though not brought into the halo through a merger, do still follow halo orbits and hence contribute to the total luminosity of it. Thus, we cannot expect a component of the halo excluding these stars to still reach its total luminosity assigned at the start of the simulation. Even though Deason et al. (2023) stress the influence of the starting luminosity, it is reassuring to find that the MDF decompose module does not fit a luminosity-spectrum just for the sake of fitting a number of galaxies that add up to the initial estimate of the luminosity.

Additionally, we observe that the most massive merger ($2.5 \cdot 10^8$ $M_\odot$) uncovered by the initial simulation of the entire catalogue is missing from this mass-spectrum as the most massive progenitor we recover has a mass of $1.3 \cdot 10^7$ $M_\odot$. We proposed earlier that this progenitor is GES, however, we now notice that by excluding what we believed are in-situ disc stars kicked up to halo orbits by this exact merger galaxy, we end up excluding it. This suggests that by excluding the "in-situ" stars, we inevitably exclude some accreted metal-rich stars brought in by a massive progenitor resembling GES. Therefore, in order to improve upon the exclusion of *Splash* stars that pollute the halo catalogue, it would be beneficial to look at a quantity that

can differentiate between in-situ halo stars and those brought in by galaxy mergers. As a result of slower chemical evolution in dwarf galaxies, at a given [Fe/H], dwarf galaxies have a lower [α/Fe] compared to that of the Milky Way (e.g. Tolstoy et al. 2009). Hence, by comparing the alpha-to-iron abundance of the metal-rich Gaussian in our catalogue, we could potentially differentiate the in-situ from the accreted component of stars. Indeed, Helmi et al. (2018) find that there is a significant difference between the GES stars and those belonging to the thin and thick disc. With this approach, we could properly exclude the kicked-up disc stars and create a clean sample of purely accreted halo stars, hence this is a major step for future research on this topic, once more alpha abundances are available.

In addition to excluding GES, by excluding the stars that were initially thought to be kicked-up thick disc stars, we likely also exclude more accreted stars. As was discussed in 4.2, we found that a fraction of stars belonging to the Sagittarius dwarf galaxy are probably part of this "in-situ" component. Hence, we once again underline that the decomposition of the halo stars into three Gaussian components is not an ideal method of studying the halo and should not be used to infer concrete results, but aid in their interpretation.

4.3.2.2 Offset to the MZR

As well as modelling the mass-spectrum using the Kirby et al. (2013) MZR shown in eq. 1, we model an additional spectrum using a -0.3 dex offset to the MZR proposed by Naidu et al. (2022) to better describe the relationship between mass and metallicity for destroyed dwarf galaxies that fully mixed with the halo. It is visible from the right panel of Figure 19 that the cumulative profile of this relation (orange line) results in a larger number of accreted galaxies compared to the result of the Kirby et al. (2013) MZR (purple line), particularly up to 10^5 $M_\odot$ and above 10^6 $M_\odot$. Similarly, Deason et al. (2023) find that the offset results in a higher estimate of galaxies with larger masses. It is evident that the bias towards lower metallicities created by the -0.3 dex offset results in the estimation of a larger number of massive progenitors. Nevertheless, even using the Naidu et al. (2022) relation, we still do not recover GES in this subsample of stars. As expected, we find that the stellar mass and luminosity estimated by this relation is higher than what we previously found: $(2.8 \pm 0.9) \cdot 10^8$ $M_\odot$ and $(1.8 \pm 0.6) \cdot 10^8$ $L_\odot$.

Kirby et al. (2013) acknowledge that their MZR might not be entirely reliable in the metal-poor part of the metallicity distribution as a result of selection biases in the sample used to determine the relation. Therefore, biasing the relation towards lower metallicities is already an improvement. However, even the Naidu et al. (2022) relation might still suffer selection biases, hence a future direction of this work could include determining an MZR that is reliable down to the extremely metal-poor end of the metallicity distribution which can probe even the smallest of the dwarf galaxies. Another future improvement of this work would be applying the Naidu et al. (2022) offset to the entire halo catalogue to inspect how the offset and the non-Gaussianity of the sample could impact the result. Due to the systems update mentioned earlier, we were not able to execute this step. We discuss the reasons why more deeply in the Appendix. Nevertheless, we underline the importance of this step as it could provide us with a greater understanding of the merger history of the halo, especially for a sample of stars for which the kicked-up disc component is cleanly removed without eliminating the GES stars.

5 Conclusion

In this project, we perform a chemical analysis of the Milky Way halo and create a mass-spectrum of its progenitors. We build from the work of Deason et al. (2023) and implement their statistical method of decomposing the metallicity composition of the halo based on the assumption that the MDF of a galaxy can be decomposed into smaller Gaussian MDFs of its progenitors. We use a homogeneous sample of halo stars created by cross-matching the Pristine DR1 and deeper proprietary metallicity values (Martin et al., 2023) to an RPM catalogue (Viswanathan et al., 2023) that specifically selects stars with halo-like orbits. In this way, we improve upon their previous work as we implement a larger and homogeneous sample with high-quality [Fe/H] measurements of 294,015 stars (after quality cuts).

We start our investigation of the chemical composition of the halo by using a Gaussian mixture method that fits multiple Gaussian functions to the MDF of the catalogue. We divide it into 33 regions and find that most regions can be decomposed into three Gaussian components: a metal-rich one that we interpret as the kicked-up disc component, a more metal-poor component interpreted as the accreted halo component and lastly a very metal-poor tail. In general, we find that the metallicity of the halo decreases with distance. Furthermore, we find a particularly metal-rich region of the most metal-rich component of the catalogue in the $-50° < l < 50°$ range, especially in the $9 - 20$ kpc galactocentric distance bin. Based on a simulation of the Sagittarius in the Milky Way and LMC potential (Vasiliev et al., 2021), we determine that an older wrap of the Sagittarius dwarf galaxy stripped about 2.5 Gyr ago is causing the increase in the metallicity of this region. In addition to this, we find a slight difference in the metallicity of the northern and southern galactic halo, likely attributable to the Sagittarius stream depositing its stars in the northern hemisphere. Lastly, we locate an overdensity of stars around $l = -100°$ and $b = 60°$ which we conclude is the Virgo Overdensity based on its metallicity and position.

We use the MDF decomposition method (Deason et al., 2023) to model 33 regions of the halo as if they are representative of it as a whole. From this, we find that the progenitor history of the Milky Way is not isotropic for the entire halo and that it likely endured various mergers that are not fully mixed. We also conclude that this method is sensitive to small differences in chemical composition, hence choosing a sample of stars that adequately represents the halo is crucial. We find that for most regions along $60° <| l |< 180°$, merger galaxies with masses about $10^4 - 10^6$ $M_\odot$ dominate the mass-spectrum by number, while the rest of the footprint of the catalogue is dominated by progenitors with masses $\lesssim 10^4$ $M_\odot$. Additionally, we recover a single most massive merger ($10^{7.5} - 10^8$ $M_\odot$) in all the region mass-spectra. Using the complete sample of 294,015 stars, we recover the total luminosity- and mass-spectrum of the dwarf galaxies which compose the halo whose pericentre is located inside $4-20$ kpc from the galactic centre. From this, we determine that the halo was composed of ~ 6000 small galaxies ($10^2 < M_\odot < 10^5$) comparable to Canes Venatici, Hercules and Ursa Major and ~ 50 massive galaxies ($10^6 < M_\odot < 10^8$) comparable to Sculptor, Fornax and WLM, while the most massive merger we recover has the mass of $2.5 \cdot 10^8$ $M_\odot$, which agrees with recent estimates of the GES merger (Naidu et al. 2021, Lane et al. 2023). Deason et al. (2023) also recover a merger of similar size. From these results, we estimate the mass of the halo to be $(6.1 \pm 2.1) \cdot 10^8$ $M_\odot$. As our catalogue probes the halo only up to a galactocentric distance of 20 kpc, we note that as for the mass-spectrum, this result is better understood as a mass estimate of stars that were brought in by dwarf galaxies whose pericentre is inside this radius. Hence, a future improvement of this work could include the use of a halo sample spanning a larger distance from the galactic centre.

We note the possibility that our sample includes a fraction of in-situ disc stars kicked to eccentric halo-like orbits by the GES merger 10 Gyr ago. Therefore, we create an additional subset of stars by statistically excluding a fraction of the most metal-rich ones. This results in a subset half the initial size, with an almost Gaussian MDF. By applying the MDF decomposition module to this sample, we find that it was composed of $\sim$ 3000 small galaxies ($10^2 < M_\odot < 10^4$) and 10 massive galaxies ($10^6 < M_\odot < 10^7$). As we now model a sample that excludes a significant fraction of stars on halo-like orbits, we also cannot expect to recover the total mass of the halo. We estimate the mass of this purely accreted halo sample to be $(5.0 \pm 1.7) \cdot 10^7$ $M_\odot$, whose stars were, once again, brought in by galaxies with pericentres inside the 20 kpc radius of the Milky Way. By excluding the possibly "in-situ disc stars", we do not recover the most massive merger, comparable in size to GES. This means that by excluding the metal-rich Gaussian component of our catalogue we not only exclude in-situ stars but likely also some stars accreted stars. Hence, we underline another crucial step for future work: differentiating between in-situ stars and GES stars by comparison of alpha-to-iron abundances, as was demonstrated by Helmi et al. (2018).

For both samples of the halo, we find a few thousand faint/small mergers ($M_V \gtrsim -10$) and less than 50 luminous/massive ones. Compared to previous work on this topic (Deason et al., 2023), we record an increase in faint mergers of over 10 times. We attribute this result to a metallicity-sensitive sample that is fit to probe even the smallest dwarf galaxies accreted by the Milky Way halo. It should be noted that authors of the MDF decomposition module warn that due to the assumption of Gaussian MDFs, the overestimation of smaller dwarf galaxies is likely. However, with either of the samples of stars, we uncover thousands of faint mergers, hence we conclude that this increase in the number of small galaxies is a result of the catalogue which represents the MDF well, even down to the very metal-poor regime. Additionally, we model the subset of stars excluding the metal-rich Gaussian component using a -0.3 dex offset to the Kirby et al. (2013) MZR, postulated by Naidu et al. (2022) to better represent the relationship between mass and metallicity for destroyed dwarf galaxies. We find that this relation estimates a larger number of massive progenitors compared to the Kirby et al. (2013) relation.

While we significantly improved upon the previous results of this method by using a larger and homogeneous set of stars that probes the lowest scale of galaxy formation, we note that there is still room for future improvement. By using an even larger halo sample with precise and accurate metallicities that span the entirety of the halo, we could uncover more peculiarities in the build-up of the halo with more certainty. This would also decrease the chances of some results being impacted by the statistics of small numbers, as we found was the case for the Gaussian mixture method. Moreover, the inclusion of a larger number of stars would statistically better represent the halo MDF. Lastly, we find that the MDF decomposition method is very sensitive to the version of imported packages it uses and to the change of the parameter `npar` which assigns the number of luminosity bins of progenitor galaxies. Therefore, it would be beneficial for future work to investigate what is causing these issues and if they bias the result in any way.

We have demonstrated in this work that while there are likely a few tens of encounters with massive mergers in the history of the Milky Way, the mass-spectrum of the galactic halo is certainly dominated by thousands of small dwarf galaxies. In this way, we have gained more insight into the composition of the Milky Way halo. As the old Croatian proverb states: *"Zrno po zrno pogača, kamen po kamen palača"*, which literally translates to "Seed by seed -bread, stone by stone -palace", we too find that one of the largest components of the Milky Way is mostly composed of the smallest dwarf galaxies.

6 Acknowledgements

Firstly, I would like to thank my supervisor Else Starkenburg. Her helpful advice, patient guidance and kind words of encouragement inspired me to continue giving my best efforts even in moments when that did not seem possible. She is truly a wonderful and inspiring person to work with. I am grateful that I had this experience.

Secondly, I want to thank Akshara Viswanathan for kindly letting me build up from her previous work by providing me with the Pristine DR1 and RPM catalogue used throughout this work, a notebook of code to help start the analysis and helpful comments about improving this work.

I would also like to thank Martin Vogelaar and the rest of the computer group at the Kapteyn Institute for helping me in the process of running simulations. Martin was always open to questions and gave helpful suggestions on how to create more efficient code and shorten its runtime. His encouraging words motivated me to continue.

Finally, I would like to thank George-Luca Iconaru for being by my side throughout the completion of this thesis. Luca showed continual support and listened to me whenever I wanted to sort my ideas out loud, proofread my thesis and encouraged me when I needed it most.

References

Abolfathi, B., Aguado, D. S., Aguilar, G., Allende Prieto, C., et al. (2018). The Fourteenth Data Release of the Sloan Digital Sky Survey: First Spectroscopic Data from the Extended Baryon Oscillation Spectroscopic Survey and from the Second Phase of the Apache Point Observatory Galactic Evolution Experiment. *ApJS*, 235(2):42.

Aguado, D. S., Youakim, K., González Hernández, J. I., Allende Prieto, C., et al. (2020). Erratum: The Pristine survey - VI. The first three years of medium-resolution follow-up spectroscopy of Pristine EMP star candidates. *MNRAS*, 491(4):5299–5299.

Balbinot, E. and Helmi, A. (2021). Linking nearby stellar streams to more distant halo overdensities. *A&A*, 654:A15.

Beers, T. C. and Christlieb, N. (2005). The Discovery and Analysis of Very Metal-Poor Stars in the Galaxy. *ARA&A*, 43(1):531–580.

Belokurov, V., Erkal, D., Evans, N. W., Koposov, S. E., et al. (2018). Co-formation of the disc and the stellar halo. *MNRAS*, 478(1):611–619.

Belokurov, V., Sanders, J. L., Fattahi, A., Smith, M. C., et al. (2020). The biggest splash. *MNRAS*, 494(3):3880–3898.

Blijleven, D. B. J. (2023). *Data and error analysis for Physics Lab: skills*. For exclusive use of within the Department of Physics of the University of Groningen.

Buder, S., Sharma, S., Kos, J., Amarsi, A. M., et al. (2021). The GALAH+ survey: Third data release. *MNRAS*, 506(1):150–201.

Davé, R. (2008). The galaxy stellar mass-star formation rate relation: evidence for an evolving stellar initial mass function? *MNRAS*, 385(1):147–160.

Deason, A. J. and Belokurov, V. (2024). Galactic Archaeology with Gaia. *arXiv e-prints*, page arXiv:2402.12443.

Deason, A. J., Belokurov, V., and Sanders, J. L. (2019). The total stellar halo mass of the Milky Way. *MNRAS*, 490(3):3426–3439.

Deason, A. J., Koposov, S. E., Fattahi, A., and Grand, R. J. J. (2023). Unravelling the mass spectrum of destroyed dwarf galaxies with the metallicity distribution function. *MNRAS*, 520(4):6091–6103.

Dodd, E., Callingham, T. M., Helmi, A., Matsuno, T., et al. (2023). Gaia DR3 view of dynamical substructure in the stellar halo near the Sun. *A&A*, 670:L2.

Drlica-Wagner, A., Bechtol, K., Mau, S., McNanna, M., et al. (2020). Milky way satellite census. i. the observational selection function for milky way satellites in des y3 and pan-starrs dr1. *ApJ*, 893(1):47.

Gaia Collaboration, Vallenari, A., Brown, A. G. A., Prusti, T., et al. (2023). Gaia Data Release 3. Summary of the content and survey properties. *A&A*, 674:A1.

Helmi, A. (2020). Streams, Substructures, and the Early History of the Milky Way. *ARA&A*, 58(1):205–256.

Helmi, A., Babusiaux, C., Koppelman, H. H., Massari, D., et al. (2018). The merger that led to the formation of the Milky Way's inner stellar halo and thick disk. *Nature*, 563(7729):85–88.

Helmi, A. and White, S. D. M. (1999). Building up the stellar halo of the Galaxy. *MNRAS*, 307(3):495–517.

Ibata, R., Malhan, K., Tenachi, W., Ardern-Arentsen, A., et al. (2024). Charting the Galactic Acceleration Field. II. A Global Mass Model of the Milky Way from the STREAMFINDER Atlas of Stellar Streams Detected in Gaia DR3. *ApJ*, 967(2):89.

Ibata, R. A., Gilmore, G., and Irwin, M. J. (1994). A dwarf satellite galaxy in Sagittarius. *Nature*, 370(6486):194–196.

Jurić, M., Ivezić, Ž., Brooks, A., Lupton, R. H., et al. (2008). The Milky Way Tomography with SDSS. I. Stellar Number Density Distribution. *ApJ*, 673(2):864–914.

Kirby, E. N., Cohen, J. G., Guhathakurta, P., Cheng, L., et al. (2013). The Universal Stellar Mass-Stellar Metallicity Relation for Dwarf Galaxies. *ApJ*, 779(2):102.

Kirby, E. N., Lanfranchi, G. A., Simon, J. D., Cohen, J. G., et al. (2011). Multi-element Abundance Measurements from Medium-resolution Spectra. III. Metallicity Distributions of Milky Way Dwarf Satellite Galaxies. *ApJ*, 727(2):78.

Koppelman, H., Helmi, A., and Veljanoski, J. (2018). One Large Blob and Many Streams Frosting the nearby Stellar Halo in Gaia DR2. *ApJL*, 860(1):L11.

Koppelman, H. H. and Helmi, A. (2021). The reduced proper motion selected halo: Methods and description of the catalogue. *A&A*, 645:A69.

Koppelman, H. H., Helmi, A., Massari, D., Roelenga, S., and Bastian, U. (2019). Characterization and history of the Helmi streams with Gaia DR2. *A&A*, 625:A5.

Kunder, A., Kordopatis, G., Steinmetz, M., Zwitter, T., et al. (2017). The Radial Velocity Experiment (RAVE): Fifth data release. *AJ*, 153(2):75.

Lane, J. M. M., Bovy, J., and Mackereth, J. T. (2023). The stellar mass of the Gaia-Sausage/Enceladus accretion remnant. *MNRAS*, 526(1):1209–1234.

Leaman, R. (2012). Insights into Pre-enrichment of Star Clusters and Self-enrichment of Dwarf Galaxies from Their Intrinsic Metallicity Dispersions. *AJ*, 144(6):183.

Majewski, S. R., Schiavon, R. P., Frinchaboy, P. M., Allende Prieto, C., et al. (2017). The Apache Point Observatory Galactic Evolution Experiment (APOGEE). *AJ*, 154(3):94.

Majewski, S. R., Skrutskie, M. F., Weinberg, M. D., and Ostheimer, J. C. (2003). A Two Micron All Sky Survey View of the Sagittarius Dwarf Galaxy. I. Morphology of the Sagittarius Core and Tidal Arms. *ApJ*, 599(2):1082–1115.

Martin, N. F., Starkenburg, E., Yuan, Z., Fouesneau, M., et al. (2023). The Pristine survey – XXIII. Data Release 1 and an all-sky metallicity catalogue based on Gaia DR3 BP/RP spectro-photometry. *arXiv e-prints*, page arXiv:2308.01344.

McConnachie, A. W. (2012). The observed properties of dwarf galaxies in and around the local group. *AJ*, 144(1):4.

Nadler, E. O., Wechsler, R. H., Bechtol, K., Mao, Y.-Y., et al. (2020). Milky way satellite census. ii. galaxy–halo connection constraints including the impact of the large magellanic cloud. *ApJ*, 893(1):48.

Naidu, R. P., Conroy, C., Bonaca, A., Zaritsky, D., et al. (2021). Reconstructing the Last Major Merger of the Milky Way with the H3 survey. *ApJ*, 923(1):92.

Naidu, R. P., Conroy, C., Bonaca, A., Zaritsky, D., et al. (2022). Live Fast, Die α-Enhanced: The Mass-Metallicity-α Relation of the Milky Way's Disrupted Dwarf Galaxies. *arXiv e-prints*, page arXiv:2204.09057.

Nepal, S., Chiappini, C., Queiroz, A. B. A., Guiglion, G., et al. (2024). Discovery of the local counterpart of disc galaxies at z $>$ 4: The oldest thin disc of the Milky Way using Gaia-RVS. *arXiv e-prints*, page arXiv:2402.00561.

Pedregosa, F., Varoquaux, G., Gramfort, A., Michel, V., et al. (2011). Scikit-learn: Machine learning in Python. *Journal of Machine Learning Research*, 12:2825–2830.

Perottoni, H. D., Limberg, G., Amarante, J. A. S., Rossi, S., et al. (2022). The Unmixed Debris of Gaia-Sausage/Enceladus in the Form of a Pair of Halo Stellar Overdensities. *ApJL*, 936(1):L2.

Python Software Foundation (2022). multiprocessing — Process-based parallelism. https://docs.python.org/3/library/multiprocessing.html. Accessed: June 2024.

Speagle, J. S. (2020). dynesty: a dynamic nested sampling package for estimating Bayesian posteriors and evidences. *MNRAS*, 493(3):3132–3158.

Starkenburg, E., Martin, N., Youakim, K., Aguado, D. S., et al. (2017). The Pristine survey - I. Mining the Galaxy for the most metal-poor stars. *MNRAS*, 471(3):2587–2604.

Tolstoy, E., Hill, V., and Tosi, M. (2009). Star-formation histories, abundances, and kinematics of dwarf galaxies in the local group. *ARA&A*, 47(1):371–425.

Vasiliev, E., Belokurov, V., and Erkal, D. (2021). Tango for three: Sagittarius, LMC, and the Milky Way. *MNRAS*, 501(2):2279–2304.

Viswanathan, A., Starkenburg, E., Koppelman, H. H., Helmi, A., et al. (2023). Hidden deep in the halo: selection of a reduced proper motion halo catalogue and mining retrograde streams in the velocity space. *MNRAS*, 521(2):2087–2102.

Viswanathan, A., Yuan, Z., Ardern-Arentsen, A., Starkenburg, E., et al. (2024). The Pristine survey – XXVI. The very metal-poor Galaxy: Chemodynamics through the follow-up of the Pristine-Gaia synthetic catalogue. *arXiv e-prints*, page arXiv:2405.13124.

Vivas, A. K., Zinn, R., Farmer, J., Duffau, S., et al. (2016). Disentangling the Virgo Overdensity with RR Lyrae stars. *ApJ*, 831(2):165.

Willmer, C. N. A. (2018). The Absolute Magnitude of the Sun in Several Filters. *ApJS*, 236(2):47.

Yanny, B., Rockosi, C., Newberg, H. J., Knapp, G. R., et al. (2009). SEGUE: A spectroscopic survey of 240,000 stars with g = 14-20. *AJ*, 137(5):4377–4399.

Youakim, K., Starkenburg, E., Aguado, D. S., Martin, N. F., et al. (2017). The Pristine survey - III. Spectroscopic confirmation of an efficient search for extremely metal-poor stars. *MNRAS*, 472(3):2963–2974.

Zhao, G., Zhao, Y.-H., Chu, Y.-Q., Jing, Y.-P., et al. (2012). LAMOST spectral survey — An overview. *Research in Astronomy and Astrophysics*, 12(7):723–734.

7 Appendix

While working on this project, we have encountered some inconsistencies in the MDF decompose module by Deason et al. (2023). In this section, we will cover the more technical findings and issues. We will also include our results of a test MDF decomposition of Fornax, a classical dwarf galaxy of the Milky Way, for which the authors also showcase their results.

7.1 Version of imported packages

Throughout this work, we have mentioned that different versions of imported packages used by the MDF decomposition function greatly impact the results. The bulk of the results had been carried out prior to a systems update that changed the versions of `dynesty` and `SciPy`. While different from the results of Deason et al. (2023), our results prior to the update looked reliable and agreed with the literature. However, after the systems update, the method started producing very curious results that do not seem to be supported by other literature findings. In Figure 20, we show the result for the complete catalogue described in 2.1. The left panel shows the mass-spectrum created after the system update. It is clear that it differs from the result on the right and estimates very few galaxies. Therefore, due to the unphysicality of the results, we decided to continue our analysis using the results created prior to the update with package versions which are likely similar to the ones used by Deason et al. (2023). Consequently, we were also not able to model the complete catalogue of the halo using the Naidu et al. (2022) offset to the MZR, as the system update interrupted the modelling.

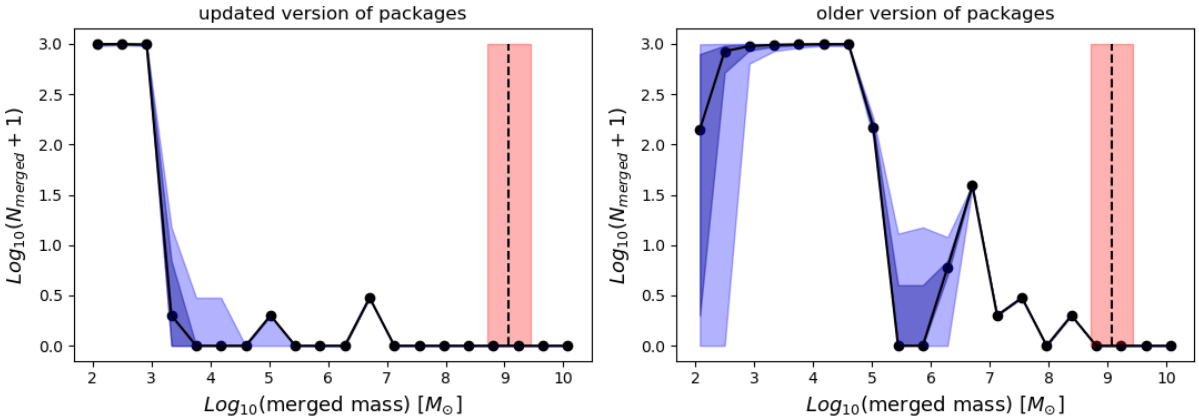

Figure 20: Comparison of results of the MDF decomposition module for the entire halo. The left panel shows the results of the complete halo catalogue made after the update of the packages, while the right panel shows those made before the update. The horizontal axes show the logarithm of the mass of merged progenitors, while the vertical ones show the logarithm of the number of merged galaxies, the rest of the figures are described in the same manner as the previous figures of this type. The only difference between these two is the version of Python packages used: the left figure shows the result using the recent versions available, while the right figure shows the result of the use of older packages.

However, we find a pleasantly surprising result. In Figure 21 we show the result of the entire halo sample using the most recent versions of packages available to us on `anaconda 2023.03` on the left and a result made with an older version of `dynesty` and `SciPy` (specifically 1.7.1 instead of 1.13.0). Evidently, there is a difference in the results, as the right panel estimates a

few more massive mergers and a few less less-massive mergers compared to the left panel, but the difference in results is not nearly as drastic as those in Figure 20. Therefore, we accept this small discrepancy as it allows us to still model the Naidu et al. (2022) MZR and investigate how it impacts the result. We find that the outcomes follow those of Deason et al. (2023).

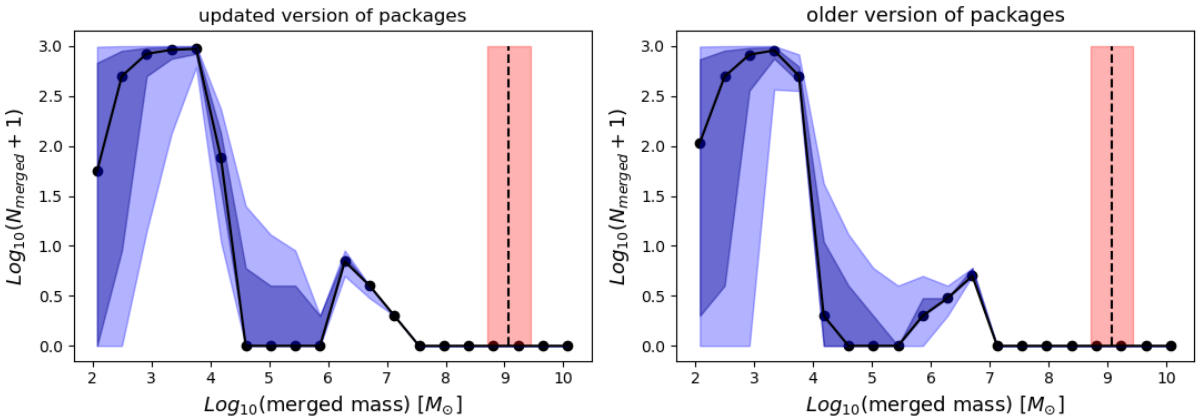

Figure 21: Comparison of results of the MDF decomposition module for the subset of stars excluding the ones belonging to the metal-rich Gaussian. The rest of the figure is analogous to that of Figure 20.

As the two samples of stars only differ in the shape of their MDFs, we conclude that this is the most likely culprit for the divergence of results prior to and after the update. We are reminded that the MDF decomposition module expects a Gaussian MDF. The complete halo catalogue clearly does not resemble this shape, but the smaller subset of stars does. Hence, we determine that the non-Gaussianity of the sample is the main cause of this discrepancy and that newer package versions are more sensitive and likely have an issue adapting to it.

7.2 Number of luminosity bins

As mentioned earlier, we find that one of the largest inconsistencies of this method is the parameter `npar` which assigns the number of luminosity bins of the simulation. If no value is assigned, the module will create 1 mag-sized luminosity bins up to 2.5 magnitudes brighter than the given estimate of the galaxy. While we find that the result stays unchanged whether the code assigns this value itself or we input it, we do find significant differences when this value is changed. In Figure 22 we show a comparison of results for Fornax, one of the dwarf galaxies presented by Deason et al. (2023). We see that the result varies significantly, which is concerning given that there is only a small difference between the number of bins. It should be noted that our result with 16 luminosity bins is much closer to those presented by the author compared to the outcome of 14 bins. However, we do find that the results are still slightly different and we attribute this to the use of different versions of Python modules, between us and the original authors. This is also the reason why the results from Figure 13 differ from this one. Figure 22 was created after the systems update mentioned above.

Because Deason et al. (2023) mention that they use 1 mag-sized bins, and find reasonable results, we adopt this size as well and believe our results too. We do not find any obvious cause for this discrepancy, however, we strongly encourage the inspection of the cause of it in the future as it could be biasing the result in some unapparent way.

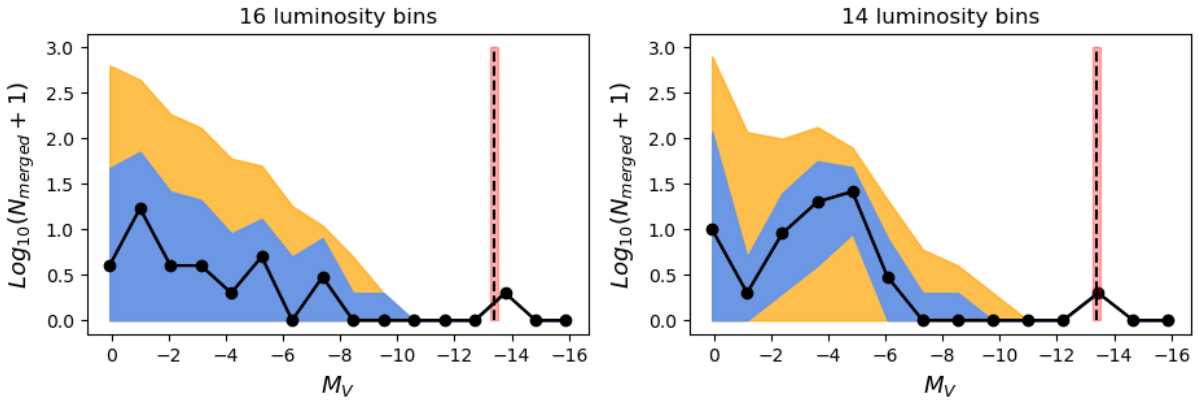

Figure 22: Comparison test of parameter `npar` for the Fornax satellite galaxy. The vertical axes of both figures show the logarithm of the number of galaxies offset by 1, while the horizontal axes show the absolute magnitude of the merged galaxies. The blue area shows the 18-84 percentile while the yellow area shows the 1-99 percentile. The black dotted line and the surrounding red area show the starting luminosity of Fornax and its error, which is the same for both panels. They only differ in the number of luminosity bins: the left panel has 16, while the right panel has 14 luminosity bins.

Lastly, we note that while we spent a significant amount of time trying to decode the potential causes of discrepancies in results described in this section, a more thorough dive into the statistical peculiarities of the code, that is outside the scope of this project, is necessary in order to properly describe the unusual behaviour.